

# Exploring the relationship between ~~sea-ice~~ sea ice and ~~primary production~~ phytoplankton growth in the Weddell Gyre using satellite and Argo-float data

Clara Celestine Douglas<sup>1,2</sup>, Nathan Briggs<sup>2</sup>, Peter Brown<sup>2</sup>, Graeme MacGilchrist<sup>3,4</sup>, and Alberto Naveira Garabato<sup>1</sup>

<sup>1</sup>Ocean and Earth Science, University of Southampton, Southampton, UK

<sup>2</sup>Ocean BioGeosciences, National Oceanography Centre, Southampton, UK

<sup>3</sup>Atmospheric and Oceanic Science, Princeton University, Princeton, NJ, USA

<sup>4</sup>School of Earth and Environmental Sciences, University of St Andrews, St Andrews, UK

**Correspondence:** Clara Douglas (C.C.Douglas@soton.ac.uk)

**Abstract.** Some of the highest rates of primary production across the Southern Ocean occur in the seasonal ice zone (SIZ), making this ~~area of prominent~~ a prominent area of importance for both local ecosystems and the global carbon cycle. There, the annual advance and retreat of ice impact light and nutrient availability, as well as the circulation and stratification, thereby imposing a dominant control on phytoplankton growth. In this study, the drivers ~~and variability of net primary production~~ (NPP) in of variability in phytoplankton growth between 2002-2020 in the Weddell Gyre SIZ were assessed using satellite ~~and autonomous biogeochemical float data~~ net primary production (NPP) products alongside chlorophyll-a and particulate organic carbon (POC) data from autonomous biogeochemical floats. Although the highest daily rates of NPP are consistently observed in the continental shelf region (water depths shallower than 2000m), the open ocean region's larger size and longer ice-free season mean that it dominates biological carbon uptake within the Weddell Gyre, accounting for ~~95~~ 93-96% of the Gyre basin's total annual NPP. Variability in the summer maximum ice-free area is the strongest predictor of inter-annual variability in total NPP across the Weddell Gyre (~~R<sup>2</sup>=62%~~), with greater ice-free area resulting in greater annual NPP, explaining nearly half of the variance (R<sup>2</sup>=42%). In the shelf region, the return of sea-ice cover controls the end of the productive season. In the open ocean, however, both satellite NPP and float data show that a decline in NPP occurs before the end of the ice-free season (~80 to ~~120-130~~ days after sea-ice retreat), ~~suggesting~~ Evidence of concurrent increases in float-observed chlorophyll-a and POC suggest that, later in the summer season, additional factors such as ~~nutrient availability limit~~ micro-nutrient availability or top-down controls (e.g. grazing) could be limiting NPP. These results indicate that in a warmer and more ice-free Weddell Gyre, notwithstanding compensating changes in nutrient supply, NPP is likely to be enhanced only up to a certain limit of ice-free days.

## 1 Introduction

20 The seasonal ice zone (SIZ) in the Southern Ocean (SO) plays an important but poorly quantified role in the net uptake and sequestration of carbon into the oceans on a range of timescales (Sigman et al., 2010; Brown et al., 2015; Van Heuven et al.,

2014; Bushinsky et al., 2019). In this region, some of the highest rates of primary production across the SO are observed (Arrigo et al., 2008b). Consequently, biological activity is considered to be key in determining the region's net carbon sink via the biological carbon pump (Brown et al., 2015; MacGilchrist et al., 2019; Henley et al., 2020). The biological carbon pump begins with the fixation of carbon through photosynthesis by phytoplankton, which lowers the levels of carbon dioxide in the surface ocean, driving uptake of carbon into the ocean from the atmosphere (Hauck et al., 2015). The fate of this fixed carbon (recycled in the surface ocean by heterotrophs or exported to depth) determines the strength and sign of the SO carbon sink (Arteaga et al., 2019; Ducklow et al., 2018; Sigman et al., 2010; Boyd et al., 2019). Furthermore, primary production forms the base of a rich and efficient food web in the SIZ, with high productivity regions supporting areas of ecological significance (Hindell et al., 2020), and commercially important species including krill, toothfish and squid (Trebilco et al., 2020).

Sea-ice dynamics play a critical role in primary production in the SIZ by attenuating light and altering stratification, mixing, and nutrient delivery (McGillicuddy et al., 2015; Gupta et al., 2020; Twelves et al., 2021). ~~Much of~~ Many observational (e.g. Arteaga et al., 2020; Bisson and Cael, 2021; Hague and Vichi, 2021; von Berg et al., 2020; Giddy et al., 2023; Briggs et al., 2018; U and model-based (e.g. Schultz et al., 2021; Taylor et al., 2013; Briggs et al., 2018; Twelves et al., 2021; McGillicuddy et al., 2015; Gupta et al., 2020) studies have enhanced our understanding of these impacts ~~is derived from regional, small-scale, and modeling studies (e.g. Bisson and Cael, 2021; von Berg et al., 2020; Giddy et al., 2023; Briggs et al., 2018; Twelves et al., 2021; McGillicuddy et al., 2015; Gupta et al., 2020) on regional (SO-wide) scales and at small, local scales.~~ However, ~~observational evidence for their basin-scale spatiotemporal relationship is lacking. In light of observed and anticipated changes in the climate of the SIZ (Kumar et al., 2021; Ludescher et al., 2019; Casagrande et al., 2023), the need for a deeper understanding of this relationship—and the broader controls on our understanding of the spatiotemporal relationship between sea ice and~~ net primary production (NPP) ~~in this region—is pressing on basin-scales is lacking.~~ Climate models from Coupled Model Intercomparison Project Phase 5 and 6 (CMIP5 and CMIP6) project a decline in Antarctic sea-ice area and concentration as a response to anthropogenic climate change (Casagrande et al., 2023). However, low confidence in projections, due to the complexity of ocean-ice-atmosphere systems, means that exact estimates of decline are uncertain (Casagrande et al., 2023; Meredith et al., 2019). ~~It is anticipated, therefore, that changes in primary production in the SIZ will follow in the coming decades, with~~ Therefore, in light of these observed and anticipated changes in the climate of the SIZ (Kumar et al., 2021; Ludescher et al., 2019; Casagrande et al., 2023), the need for a deeper understanding of the relationship between sea ice and NPP is pressing, as changes in sea ice will have concomitant impacts on carbon uptake and ecosystem health. However, the crucial gaps in our understanding of the drivers of NPP in the SIZ mean that large uncertainty remains about the nature and extent of these changes (Campbell et al., 2019; Henley et al., 2020; Kim and Kim, 2021; Pinkerton et al., 2021; Séférian et al., 2020; Henson et al., 2022).

The Weddell Gyre-Sea is one of a few regions of deep and bottom water formation, and it has largely been thought that the transportation of these water masses to depth was the principal pathway for vast quantities of carbon (taken up through the solubility and biological carbon pumps) to be sequestered from the SO (~~Jullion et al., 2014; Meredith et al., 2014; Van Heuven et al., 2014) (Jullion et al., 2014; Meredith et al., 2014; Van Heuven et al., 2014; Nissen et al., 2022).~~ However, it has more recently been hypothesised that this may not be the case. Instead, the Weddell Gyre's net CO<sub>2</sub> sink may be driven by biological carbon uptake in the offshore central Gyre, where the accumulation of respired carbon at mid-depths within local Circumpolar Deep Water, and circulation of this enriched water mass out of the Gyre, provide a significant pathway for carbon sequestration north

of the Gyre (MacGilchrist et al., 2019). Many SO biological carbon pump studies have focused on coastal and shelf regions, such as highly productive polynyas (e.g. McGillicuddy et al., 2015; Arrigo et al., 2015). However, the offshore (open ocean) area of the Weddell Gyre exhibits high annual NPP in comparison to shelf regions and has been documented as one of the Sea has been shown to contribute greatly to the region's annual primary production, with annual NPP in the offshore (open ocean) marginal ice zone ( $73.7 \text{ g C m}^{-2} \text{ a}^{-1}$ ) exceeding that seen in the shelf marginal ice zone ( $65.2 \text{ g C m}^{-2} \text{ a}^{-1}$ ), and almost matching the annual NPP exhibited in the shelf region ( $77.0 \text{ g C m}^{-2} \text{ a}^{-1}$ ) (Arrigo et al., 2008b). In this way, the Weddell Sea marginal ice zone was identified as the largest and most productive marginal ice zones in the Southern Ocean (Arrigo et al., 2008b) zone of all the geographic sectors investigated (25% greater than the Ross Sea marginal ice zone; Arrigo et al., 2008b). As such, the interaction between biology and circulation in the off-shore area of this SO region is particularly important, and it is vital to advance understanding of what drives these processes now to improve prediction of how they may change in the future.

Given the importance of biological carbon uptake in the Weddell Gyre for local ecosystems and the global carbon cycle, this paper characterises and quantifies the basin-scale relationship between NPP and sea-ice sea ice and phytoplankton growth using both satellite net primary production (NPP) products and *in situ* observations of chlorophyll-a (Chl-a) and particulate organic carbon (POC) from Biogeochemical (BGC) Argo floats. In Sect. 2 we describe our data and methods and highlight, as well as highlight and quantify uncertainties associated with our approach. In Sect. 3 we present a multi-year perspective of NPP in the Weddell Gyre, as well as its variability, before discussing the importance of sea-ice sea ice and nutrient availability in driving inter-annual variability in NPP in Sect. 4.

## 2 Data and Methods

### 2.1 Study Area

The Weddell Gyre is a cyclonic gyre located in the Atlantic sector of the SO (Fig. 1; Vernet et al., 2019). Water primarily enters the gyre from the east (Circumpolar Deep Water supplied from the Antarctic Circumpolar Current) and leaves toward the north, with its the Gyre's circulation and extent determined by wind forcing and topography (Hoppema, 2004; MacGilchrist et al., 2019; Vernet et al., 2019). Sea-ice Sea ice extends across almost the entire Weddell Gyre in the winter and retreats in the summer, encompassing the Gyre basin within the SIZ (Arrigo et al., 2008b; Vernet et al., 2019) (Fig. 1; Arrigo et al., 2008b; Vernet et al., 2019).

The extent of the study area was defined to align with previous studies of the Weddell Gyre (Jullion et al., 2014; Brown et al., 2015; MacC (Akhoudas et al., 2021; Jullion et al., 2014; Brown et al., 2014, 2015; MacGilchrist et al., 2019). The region is bounded by the Antarctic continent to the south and west and two hydrographic transects to the north and east: the Antarctic Deep Water Rate of Export (ANDREX) cruises, and the CLIVAR quasi-meridional I6S section at  $30^\circ \text{E}$  (Fig. 1; Bacon and Jullion, 2009; Meredith, 2010; Speer and Dittmar, 2008). For the purposes of this study, the Weddell Gyre was divided into two subregions: a shelf region (defined as the area with bathymetric depth less than 2000m) and an open-ocean region (depths greater than 2000m). The position of the 2000m isobath was extracted from TerrainBase, a 5-minute resolution global elevation database (National Geophysical Data Center/NESDIS/NOAA/U.S. Department of Commerce., 1995).

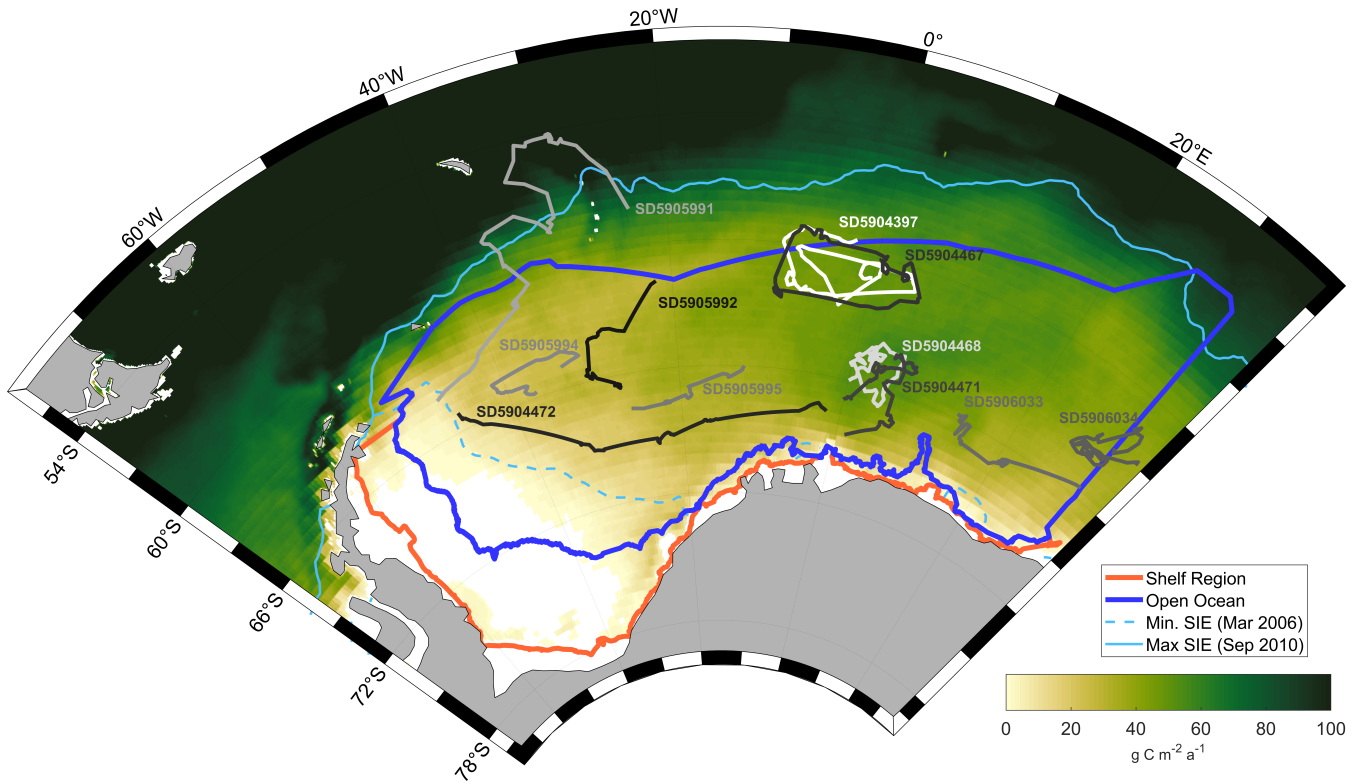


**Figure 1.** Location of the Weddell **Sea, Southern Boundary (dark blue line) Gyre** and study subregions (**dark blue**: open ocean; **green/orange**: shelf). The 18-year mean area-normalised annual NPP ( $\text{g C m}^{-2}$ ) climatology derived from MODIS-Aqua satellite measurements using the Carbon, Absorption and Fluorescence Euphotic-resolving (CAFE) model (Silsbe et al., 2016) is represented by the yellow to green colourmap. White areas represent no data (permanent **sea-ice** **sea ice** present). SOCCOM float trajectories from **12-11** BGC-Argo floats are shown in greyscale and **labeled** **labelled** with WMO ID. Profiles from float SD5905991 located north of the study region were not included in the analysis. The dashed and solid light blue lines denote the summer minimum (March 2006) and winter maximum (September 2010) sea ice extent respectively.

## 90 2.2 Satellite Data

### 2.2.1 **Sea-Ice** **Sea Ice**

Daily satellite **sea-ice** **sea ice** concentrations over 2002-2020 were taken from the NOAA/National Snow and Ice Data center (NSIDC) Climate Data Record (Version 4, Meier et al., 2021). The data were obtained on the NSIDC polar stereographic 25 x 25 km grid. Eight-day means of sea-ice concentration (SIC) were calculated to match the NPP and **Chlorophyll-a** (**Chl-a**) data  
 95 temporal resolution. Pixels were defined as ice-free if the SIC was less than 15% (Windnagel et al., 2021). Annual statistics were calculated over austral years 2003-2020, starting July 2002 and ending June 2020. The sea-ice area (SIA) was calculated

by multiplying the SIC within each pixel by its area. Ice-free area (IFA) was calculated as the difference between the total area of the Weddell Gyre (and sub-regions) and the SIA.

### 2.2.2 NPP (and Chlorophyll-a)

100 Satellite-derived NPP products calculated from MODIS (Moderate-Resolution Imaging Spectroradiometer)-Aqua chlorophyll-a (Chl-a) data were obtained from the Ocean Productivity website ([www.science.oregonstate.edu/ocean.productivity/](http://www.science.oregonstate.edu/ocean.productivity/); Oregon State University, 2019). We use the NPP product derived using the Carbon, Absorption and Fluorescence Euphotic-resolving (CAFE) model (Silsbe et al., 2016; Westberry and Behrenfeld, 2013). [The CAFE model is an absorption-based model that considers the amount of energy absorbed by phytoplankton, photoacclimation, and the efficiency with which energy](#)  
 105 [is converted into biomass. CAFE was chosen over other NPP models as it is currently the most comprehensive open-source NPP model and is the most robust in capturing the baseline productivity of the SO \(Silsbe et al., 2016; Ryan-keogh et al., 2023; Westberry et al., 2016\). The CAFE NPP product is calculated using MODIS-derived products: Chl-a, PAR \(photosynthetically available radiation\), sea surface temperature; MODIS-derived absorption and backscattering variables configured using the Generalized Inherent Optical Property \(GIOP\) model; and mixed layer depth provided by the HYbrid Coordinate Ocean Model \(HYCOM\). Input](#)  
 110 [data to the CAFE model are cloud-filled via spatial and temporal interpolation prior to calculating NPP. The data-resolution resolution of the NPP data is 8-day averages on a 1/12° latitude-longitude grid \(2-4km zonal resolution, 8-10km meridional resolution in this region\) for the period 2002-2020. The CAFE model is an absorption-based model that considers the amount of energy absorbed by phytoplankton, photoacclimation \(how much energy is used to fuel growth or is dissipated\), and the efficiency with which energy is converted into biomass. CAFE was chosen over other NPP models as it has the best performance of all the models in SO regions, as assessed in Silsbe et al. \(2016\).](#) Cloud-filled MODIS-Aqua Chl-a concentration data were also obtained at the same resolution as the NPP data [to later compare to BGC-Argo float data as proxies for growth.](#)

[Three other NPP models were analysed to assess the robustness of the CAFE results. The Carbon-based Productivity Model \(CbPM; Westberry et al., 2008; Behrenfeld et al., 2005\) relates NPP to phytoplankton carbon biomass \(derived from particulate backscatter received by MODIS-Aqua\). Both the Vertically Generalized Production Model \(VGPM; Behrenfeld and Falkowski, 2004\) and Eppley-adjusted VGPM \(eppley; Eppley, 1972\) products are calculated based on the relationship between chlorophyll and temperature derived growth rates. Eppley differs from VGPM by parameterising the relationship between temperature and phytoplankton growth rate using the positive exponential function described by Eppley \(1972\); Morel \(1991\).](#)

In our analysis, we derive a number of quantities from the basic NPP variable provided; *i.e.* the area-normalized, time-mean NPP at each lat-lon ( $x$ - $y$ ) pixel, for each 8-day period, which we label  $\mu \equiv \mu(x, y, t)$ . The spatially-averaged NPP for each subregion,  $i$ , is defined thus:

$$\bar{\mu}^{x,y}(i, t) = \frac{1}{\mathcal{A}(i, t)} \int_{\mathcal{A}(i, t)} \mu(x, y, t) dA \quad (1)$$

where  $dA \equiv dx dy$  is the area increment, and  $\mathcal{A}(i, t)$  corresponds [to](#) the areal extent of the [visible](#) ice-free area in each subregion  $i$  at time  $t$  (as ascertained from data availability in the NPP product). Note that this area is not exactly equivalent to the IFA derived from the sea-ice data [because of the "adjacency effect" of the ice edge on restricting ocean colour data](#)

130 near sea ice (Pope et al., 2017) as well as areas where there are data missing for other reasons (cloud-fill algorithm, input data: See Section 2.4). The total Weddell Gyre region corresponds to the area  $A(t) = \sum_i \mathcal{A}(i, t)$ . The annual means of the spatially-averaged NPP ( $\bar{\mu}^{x,y}$ ) are derived over the period of the austral year starting in July ( $t_s$ ) and ending in June of the following calendar year ( $t_e$ ).

The “total annual NPP” ( $N$ ) corresponds to the spatially and temporally integrated carbon uptake over each subregion:

$$135 \quad N(i, \tilde{t}) = \int_{t_s(\tilde{t})}^{t_e(\tilde{t})} \int_{\mathcal{A}(i,t)} \mu(x, y, t) dA dt \quad (2)$$

where  $\tilde{t}$  is a yearly time increment, defined over the austral year ~~starting in July ( $t_s$ ) and ending in June of the following calendar year ( $t_e$ ).~~ Although we include the time-dependence of the areal extent here for consistency, it is irrelevant in this calculation because ice-covered pixels (where  $\mu = 0$  ~~automatically contribute nothing in~~) do not contribute to the area integral. ~~Finally, we note that annual means of the spatially-averaged NPP defined above ( $\bar{\mu}^{x,y}$ ) are also derived over the period of the~~  
140 ~~austral year.~~

Ocean-colour satellite observations are restricted by the presence of ~~sea-ice~~ sea ice and when the solar angle/zenith is too low (below  $20^\circ$ , see Sect. 2.4 for more details). The number of days each pixel was visible to the ocean-colour satellite (and therefore had data recorded) was counted. For the most part, satellite-visible days are approximately equivalent to the number of days from sea-ice melt/retreat to ~~low solar angle~~ when the noontime solar zenith angle decreases to less than  $20^\circ$  and restricts  
145 ocean colour measurements.

### 2.3 Autonomous floats

We use BGC-Argo float data to evaluate the data recovery attributes of satellite data, estimate associated uncertainties (Section 2.4), and also to assess the seasonal progression of phytoplankton growth in the water column, using Chl-a as a proxy for photosynthetic potential and particulate organic carbon (POC) as a proxy for biomass. Eleven autonomous BGC-Argo floats  
150 deployed by the Southern Ocean Carbon and Climate Observations and Modelling (SOCCOM) project from 2014 onwards observed at least one complete annual cycle (from July to June) within the study region (Fig. 1). The floats were programmed to profile from 1700-2000m to the surface on 10-day intervals. ~~Data~~ Chl-a data for these floats were obtained from the 21 December 2021 SOCCOM snapshot (<https://doi.org/10.6075/J00R9PJW>) and interpolated over a 5m vertical grid. SOCCOM provide two Chl-a data products which differ in their fluorescence to Chl-a calibration. The corrected Chl-a product (*chl\_a\_corr*),  
155 which has a Southern Ocean specific correction applied (Johnson et al., 2017), was used here. Missing surface/shallow Chl-a values were extrapolated (nearest neighbor) from the shallowest data available for each profile (Appendix Fig.A1).

Mean and depth-integrated estimates of Chl-a were calculated from float profiles by integrating binned Chl-a concentrations between the surface to 200m and surface to 20m, with the mean estimates for the 0-20m bin intended to line-up with the approximate optical depth of MODIS-Aqua - i.e. what the satellites likely measured (Fig. 2; Gordon and Mc-  
160 Cluney, 1975). Under-ice profiles were identified based on criteria used in the ice avoidance algorithm, which prevents



a float ascending to the surface if the median temperature between 20-50m is less than  $-1.78^{\circ}\text{C}$  (~~Bisson and Cael, 2021~~) (Bisson and Cael, 2021; Klatt et al., 2007).

The seasonal cycles of float-observed Chl-a were assessed alongside the timings of sea-ice retreat, sea-ice return, and the date when the ~~solar-noon~~ solar zenith angle drops below  $20^{\circ}$ , restricting ocean-colour satellite observation, to get a small-scale  
165 (localised) depth-resolved perspective on the drivers of seasonal and annual Chl-a variability. The dates that floats emerged from under ice and returned to under-ice conditions were determined and the length of the ice-covered and ice-free seasons were calculated. The average latitude of each float in March was calculated, and based on this location, the date that the solar angle/zenith would be too low for MODIS-Aqua satellite coverage was determined.

POC concentrations were estimated from optical backscattering data after the removal of spikes due to large particles following (Briggs et al., 2011). "De-spiked" backscattering were averaged in 10 m bins in the upper 50 m and then at 50 m intervals to 200 m. As with the Chl-a data, missing surface/shallow backscatter values were extrapolated (nearest neighbor) from the shallowest data available for each profile. Backscatter was converted to POC concentrations using the conversion co-efficient  $3.12 \times 10^4$  as proposed in Johnson et al. (2017). The mean and depth-integrated POC in the 0-20m and 0-200m bins are reported here.

170

#### 175 **2.4 Uncertainty estimates for satellite chlorophyll-a and NPP**

Satellite estimates of annual NPP should be considered conservative due to the limitations of ocean-colour satellites and NPP products. ~~These~~ We divide these potential negative biases in satellite-derived annual NPP ~~arise due to three reasons~~ into three categories: 1) sea-ice coverage; 2) low solar angle; and 3) other data gaps.

~~Sea-ice~~ The first two we assess using BGC Argo float data. The third we assess and attempt to correct using satellite-derived sea-ice coverage data. Sea ice restricts ocean-colour satellites from viewing any production taking place under and within ~~sea-ice~~ sea ice (Arrigo and van Dijken, 2004; Peck et al., 2010; Pope et al., 2017). Spatial coverage of the ocean-colour satellite is also increasingly restricted from early March, due to the decreasing solar angle limiting optical view (Pope et al., 2017). This means that much of the surface ocean is not observed by the MODIS-Aqua satellite at the end of the summer period despite much of the region still being ice-free. It is therefore likely that some NPP is being missed at the end of the  
185 growing season. ~~As a result, NPP is considered zero during winter, where there is no satellite coverage south of  $50^{\circ}\text{S}$  due to sea-ice coverage and low solar angle~~ Finally, satellite NPP data contain additional gaps, due to a range of optical limitations, including ice adjacency cloud cover.

Without comprehensive *in situ* measurements of NPP, it is not possible to directly quantify what is missed by satellites. ~~Instead~~ However, BGC-Argo float data can be used to provide insight into these limitations, as they provide sub-surface,  
190 we ~~year-round, under-ice observations of key parameters related to NPP. Floats data have their own limitations - floats are Lagrangian autonomous observing platforms, so observations reflect both temporal and spatial variability. Additionally, sensor calibrations may vary and sensors sometimes drift towards the end of the float deployment. We did not attempt to estimate water-column integrated NPP from float data, as the floats in the study region lacked PAR (Photosynthetically Active Radiation) sensors, and, as far as we are aware, there are not yet methods for calculating NPP from float data that have been robustly~~

195 validated for widespread use. Instead, estimates of Chl-a and POC can be used as conservative proxies for phytoplankton growth/biomass to assess the importance of missed phytoplankton. While Chl-a does not directly equate to NPP, satellite Chl-a is used in all satellite NPP products, and as such we can compare float and satellite Chl-a observations. Figure 2 highlights the similarities and dissimilarities in float and satellite Chl-a estimates. The absolute values of Chl-a differ between the satellite and the float because of the way Chl-a is derived from observations on these platforms - satellite Chl-a is derived from reflectance,  
200 whereas fluorescence is used to calculate float-observed Chl-a. Nonetheless, the relative changes in Chl-a over the timeseries should be seen in both datasets. In most cases, the satellite Chl-a at each float location peaks and troughs at the same time as the float Chl-a. On some occasions, the spring peak/bloom is not fully seen by the satellites, and in several cases (Figure 2: b) and c) in 2018, f) and k) in 2020), it is missed entirely. As such, the addition of float data in this study expands on the results derived from the satellite products and allows assessment of the seasonal patterns in Chl-a. Notably, it is clear that the satellite  
205 Chl-a product does not span the entire ice-free/growing season and the floats are valuable in providing a year-round perspective on the seasonal changes in Chl-a and POC.

We use float data to determine how much of the annual-integrated Chl-a is missed and POC (in the surface 20m) is missed by satellites, reasoning that this offers a ballpark figure reasonable estimate for the fraction of missed NPP. The proportions of annual-annually integrated Chl-a and POC measured by each float observed when the float was (1) under sea-ice sea ice (using the Klatt et al. (2007) temperature criterion mentioned above) and (2) when the solar angle is less than 20°, limiting satellite  
210 view at the end of summer (from mid-March) are summarised in Table 1. At the float locations, only a small proportion of annual-annually integrated Chl-a is present under sea-ice (max 1.1% sea ice (median 10%, range 2-23%), while up to 2019% (median 9.29%) of annual-annually integrated Chl-a is observed by floats during the time when the ocean-colour satellite was unable to view the surface ocean due to low solar angle (Table 1). Up to 30% of the annually integrated POC is recorded  
215 under-ice (minimum 7%, median 19%) and an average of 12% (range 4-20%) of the surface POC is recorded after the solar angle is too low.

There are areas in the mapped NPP data where the cloud fill Ocean-colour satellites are only able to view the surface of the ocean, meaning Chl-a satellite products do not represent the full euphotic zone/water column inventory (Pope et al., 2017). The CAFE algorithm applies a light saturation model for the mixed layer and assumes a co-varying relationship between the phytoplankton absorption coefficient and light saturation below the mixed layer in order to estimate the vertical structure of Chl-a (and NPP; Silsbe et al., 2016). As a result, the subsurface Chl-a inventory may not be accurately resolved and may also miss subsurface Chl-a maximum layers, which contribute substantially to productivity and promote enhanced carbon export in the SO (Baldry et al., 2020). Again, floats enable assessment of the importance of phytoplankton missed by satellites, in this case, below 20m. The depth integrated Chl-a signal seen in Figure 2 declines later than the surface Chl-a, indicating that  
225 concentrations of Chl-a remain elevated at depth for longer than at the surface.

In addition to missing satellite NPP data under ice and at low solar zenith angle, there are further empty grid points in the mapped NPP and Chl-a data that mean that the IFA does not equate to the area of the NPP or Chl-a products where data is recorded. NPP in these areas is considered to be zero, leading to an underestimate of the regions' total NPP. Some of these gaps could be attributed to the "adjacency effect" along the ice edge and also where the cloud-fill algorithm did not complete



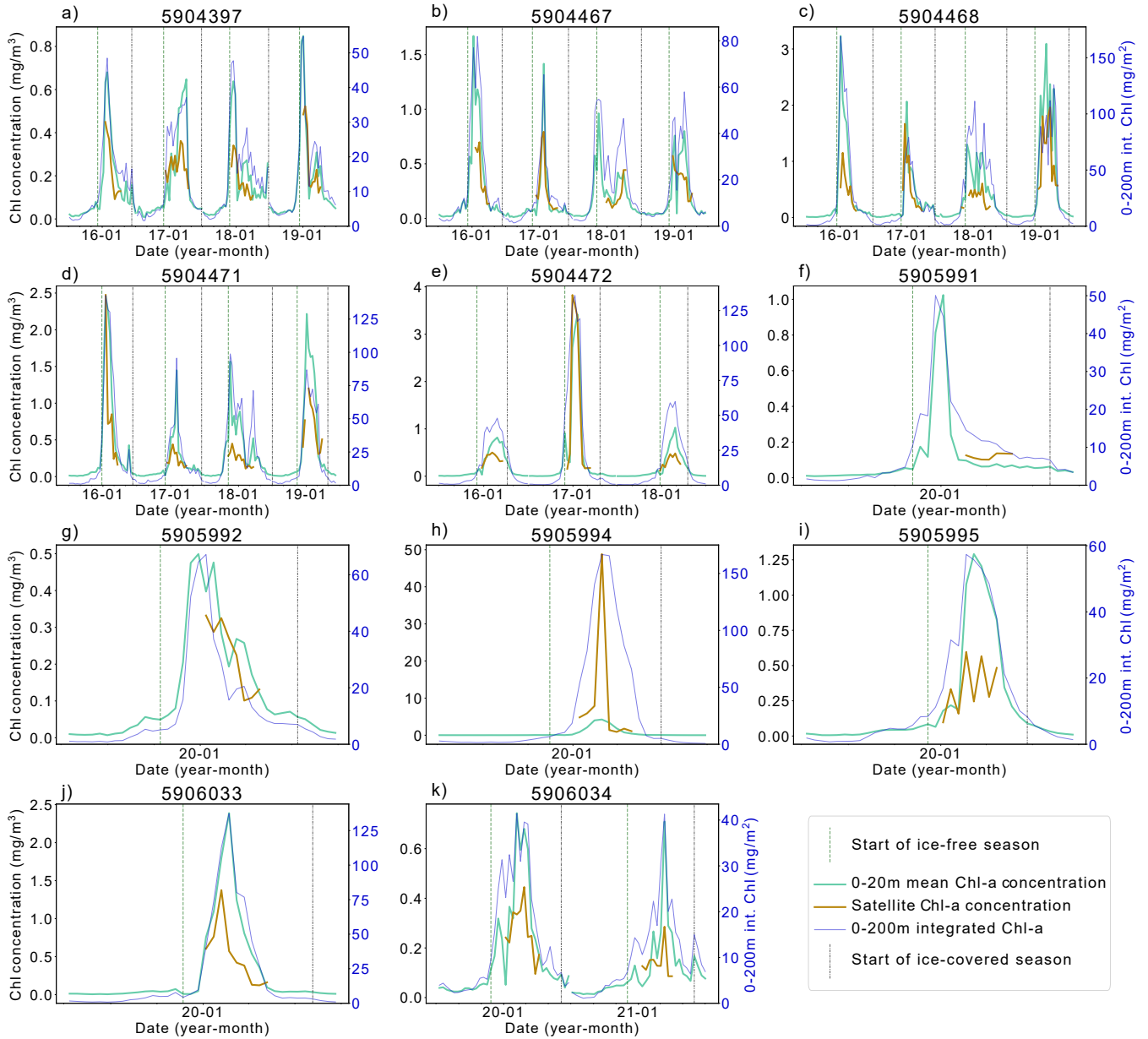


**Figure 2.** Satellite - BGC-Argo float chlorophyll-a (Chl-a) comparison. Left y-axis: mean Chl-a concentration values (1) between 0-20m (green) and (2) at the closest pixel to location of float profile (orange line). Right y-axis: the integrated Chl-a between 0-200m (dark blue line). Vertical dashed green line indicates start of ice-free season; vertical dash dot blue line indicates start of ice-season.

230 successfully ~~where data is absent despite the SIC data indicating that no sea-ice is present. There~~. In addition to this, there is also a disparity in the spatial coverage of the NPP products and the Chl-a input data used to derive CAFE NPP (Table 1). Some of the input data (absorption due to gelbstoff and detritus, absorption due to phytoplankton and backscatter spectral slope parameter) used in the CAFE algorithm to derive NPP have less extensive spatial coverage than the Chl-a input data ~~and/or don't have data along some ice edges due to satellite observation limitations~~. This means that there are some areas in the NPP product  
235 that ~~suggest imply~~ there is no NPP occurring despite Chl-a being observed by the satellite. ~~On average over a year, there is a  $7.51 \pm 3.47 \times 10^4$  km<sup>2</sup> difference in coverage between~~ Over the timeseries, between 10-100% (mean 78%, median 85%) of the area with Chl-a view and NPP data also has coverage in the CAFE NPP product (lowest values occur as the satellite view declines at the start of winter). The spatial coverage of the CAFE product in relation to IFA ranges between 0-94% over the seasonal cycle. When ice-free and with sufficient solar elevation for ocean-colour observations, on average 47% of the IFA was  
240 visible in the CAFE product. This is especially relevant for the difference between the IFA and area where NPP is observed in the CAFE product is most acute in the shelf region, where many of the 0-65% (mean 10%) of IFA has NPP data when conditions are suitable for ocean-colour observations, and many coastal polynyas that occur are visible in the input Chl-a data ; but are not translated into the NPP data. Therefore shelf integrated NPP values are expected to be underestimated. significantly underestimated. To estimate the potential total NPP occurring across the entire IFA in both the shelf and open ocean regions,  
245 data gaps were filled with the mean daily rate for each 8-day time-step within a region. As with the original calculation, the total annual NPP is then calculated by integrating the new 8-day totals for the austral year. The difference between the directly observed (raw) and imputed (gap-filled) estimates can be seen in Figure 3,b-d).

~~Ocean-colour satellites are only able to view the surface of the ocean, meaning Chl-a satellite products do not represent the full euphotic zone/water column inventory (Pope et al., 2017). The CAFE algorithm applies a light saturation model for the mixed layer and assumes a co-varying relationship between the phytoplankton absorption coefficient and light saturation below the mixed layer in order to estimate the vertical structure of Chl-a (and NPP; Silsbe et al., 2016). As a result, the subsurface Chl-a/NPP inventory may not be accurately resolved and may also miss subsurface Chl-a maximum layers, which are potentially highly productive and promote enhanced carbon export in the SO (Baldry et al., 2020). Figure 2 highlights the similarities and dissimilarities in float and satellite Chl-a estimates.~~

## 255 3 Results

### 3.1 Climatological NPP and ~~sea-ice~~Sea Ice

Total annual ~~phytoplankton~~ NPP integrated over the entire Weddell Gyre between 2003 and 2020 averaged ( $\pm$  standard deviation)  $172 \pm 34$  Tg C a<sup>-1</sup> ~~between 2003 and 2020, while annual before gap-filling and  $269 \pm 39$  Tg C a<sup>-1</sup> after gap-filling (adjusting for the missed IFA; see Section. 2.4).~~ Annual area-normalised production was on average  $97 \pm 8$  mg C m<sup>-2</sup> a<sup>-1</sup>. While the  
260 open ocean experiences lower daily rates of productivity compared to the shelf region ( $376 \pm 33$  mg C m<sup>-2</sup> d<sup>-1</sup> compared to  $582 \pm 99$  mg C m<sup>-2</sup> d<sup>-1</sup>; ~~Appendix Figure ??~~), ~~area-normalised~~ Figure 3.a), annual NPP is in fact higher per unit area in the open ocean than in the shelf region ( $97 \pm 8.2$  mg C m<sup>-2</sup> a<sup>-1</sup>,  $68 \pm 23$  mg C m<sup>-2</sup> a<sup>-1</sup> respectively; Fig. 3.A)-b). This is

**Table 1.** Estimation of ~~uncertainty in missed~~ ocean-colour satellite NPP data based on complementary BGC-Argo float data and assessment of NPP input data

Reason	Parameter	Estimate of missed data <del>Notes (%)</del>
<del>Sea-ice</del> Sea ice	<del>0</del> <u>Annual integrated Chl-a within surface (0-20m) layer</u>	<del>2 - 1.123%</del> (median <del>0.2%</del> ) <u>annual Chl-a 10%</u>
	<del>Percentage of annual Chl-a</del> <u>Annual integrated POC within surface (0-20m) layer</u>	<del>7 - 30%</del> (median <u>19%</u> )
<del>Low solar angle</del> Low solar angle	<del>0.8</del> <u>Annual integrated Chl-a within surface (0-20m) layer</u>	<del>1 - 2019%</del> (median <del>9.2%</del> ) <u>annual Chl-a 9%</u>
	<del>Percentage of annual Chl-a</del> <u>Annual integrated POC within surface (0-20m) layer</u>	<del>4 - 20%</del> (median <u>12%</u> )
<del>Missing data</del> Other data gaps	<del>7.51±3.47 x</del> <u>Fraction of IFA without NPP coverage when noon zenith angle &gt;20°.</u> <u>(Caused by a combination of the "adjacency effect" of ice edge, cloud-fill</u>	<u>Weddell Gyre: 0-94% (mean 47%)</u> <u>Shelf: 0-65% (mean 10<sup>4</sup> km<sup>2</sup> (~1.3% of WG region) %)</u>
	<del>Other data (temperature, light) used in the NPP calculation have coarser spatial coverage than Chl-a data, particularly over shelves, errors, and poor spatial coverage of input variables (absorption, backscatter)</del>	<u>Open ocean: 0-97% (mean 50%)</u>

due to a longer mean visible ice-free season. The sea-ice product shows that areas in the outer North-East edge of the open ocean are at the outer extent of the SIZ and can be ice-free for entire years, while on average, the whole open ocean region is ice-free for 139±13 days per year. The longest any of the shelf region is ice-free is 157 days, while the mean is 37±13 days. The open ocean also has a far greater area than the shelf region (50.32 x 10<sup>5</sup> km<sup>2</sup> compared to 8.81 x 10<sup>5</sup> km<sup>2</sup>, such that the open ocean represents 85% of the Weddell study region). As a result, when integrated over time and area, the open ocean accounts for a significant majority of the total carbon taken up by phytoplankton in the Weddell Gyre ~~99%±1%~~ and dominates the inter-annual variability of NPP seen in the region (Fig 3.B). ~~The~~ 3.b and c). Before imputation, the total annual NPP in the open ocean is 170±33 Tg C compared to 2±2 Tg C in the shelf region ~~-(such that the open ocean accounts for 99±1% of the total NPP in the Weddell Gyre).~~ After imputation, annual NPP rises to 255±38 Tg C a<sup>-1</sup> in the open ocean and 11±5 Tg C a<sup>-1</sup> in the shelf region. Despite seeing a large increase in shelf estimates following the use of the gap-filling approach, the

open ocean still accounts for  $96\pm 2\%$  of the imputed Weddell NPP (ranging between 93-96% depending on the NPP model chosen).

275

As described in Section. 2.4 and summarised in Table. 1, BGC Argo float estimates of Chl-a and POC both under ice and at low sun angle suggest that substantial amount of phytoplankton biomass may be missed by satellite NPP products in the open ocean (medians of 20% Chl and 39% POC for all float locations). We did not attempt to further adjust our NPP estimates for these missed data, because float biomass proxies are not directly proportional to NPP and because float coverage, while broad, was not even throughout the Weddell Gyre.

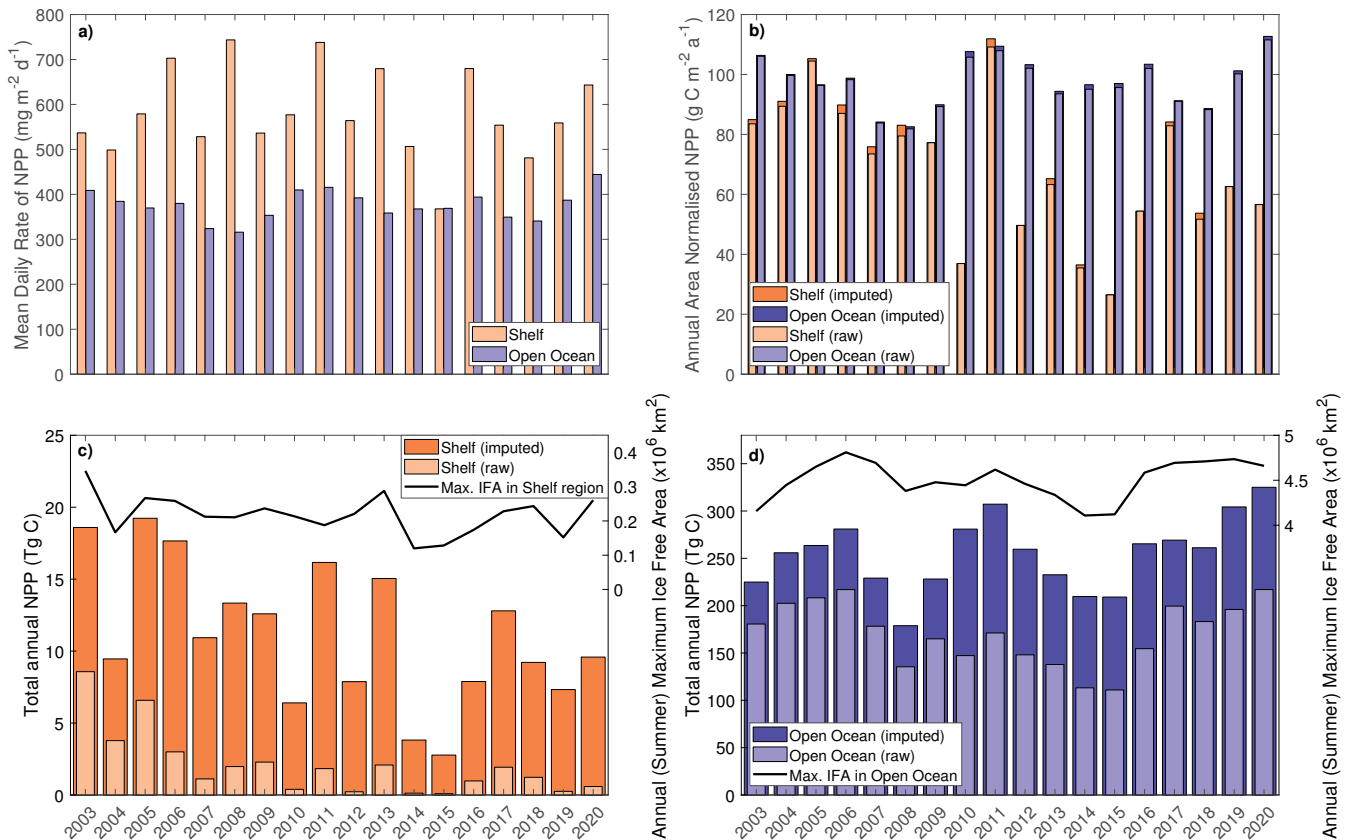


**Figure 3.** Annual-CAFE NPP: a) Mean daily NPP. Orange bars represent the shelf region value and blue bars for open ocean values; b) Area-Normalised Annual NPP; bc) Shelf Region Total Annual NPP shown on the left axis and Annual (Summer) Maximum Ice Free Area on the right axis; d) Open Ocean Total Annual NPP shown on the left axis and Annual (Summer) Maximum Ice Free Area on the right axis. The green-light bars represent the shelf region value and blue raw (directly observed) values integrated from the CAFE NPP product, the dark bars for open ocean indicate the imputed values calculated to consider data gaps in the spatial coverage of the CAFE product.

280

The summer maximum IFA for the entire Weddell Gyre averaged  $4.89 \pm 2.39$  standard deviation  $4.73 \pm 0.23 \times 10^6 \text{ km}^2$  between 2003 and 2020 (the equivalent of  $1.18 \times 10^6 \text{ km}^2$  summer sea-ice area  $80 \pm 4\%$  of the total study region). The mean IFA

per year for the entire Weddell Gyre averaged  $2.292.18 \pm 0.25-0.24 \times 10^6 \text{ km}^2$  between 2003 and 2020. On average in the shelf region, summer (maximum) IFA was  $2.392.17 \pm 0.57 \times 10^5 \text{ km}^2$  ( $25 \pm 7\%$  of the shelf area), the mean IFA was  $1.038.10 \pm 0.12$   
 285  $1.67 \times 10^{54} \text{ km}^2$ . In the open ocean region region, the average summer (maximum) IFA was  $4.50 \pm 0.22 \times 10^6 \text{ km}^2$  ( $89 \pm 4\%$  of  
 the open ocean area), mean IFA averaged  $2.08 \pm 0.23 \times 10^6 \text{ km}^2$ .

A clear seasonal cycle is seen in both NPP and IFA (Fig. 4). When comparing the mean annual cycle of open water area and total NPP, the rise in NPP coincides with the retreat of sea-ice-sea ice and increase in the area of ice-free water (Fig. 4). In the shelf region, the peak in NPP occurs at maximum open water area, and the decline in NPP coincides with the formation of sea-ice. However, in the open ocean region, NPP both regions, NPP peaks before the maximum open water area is seen and  
 290 then declines despite the continued expansion of open water, creating a mismatch between NPP and sea-ice coverage trends of NPP and ice-free area from February.

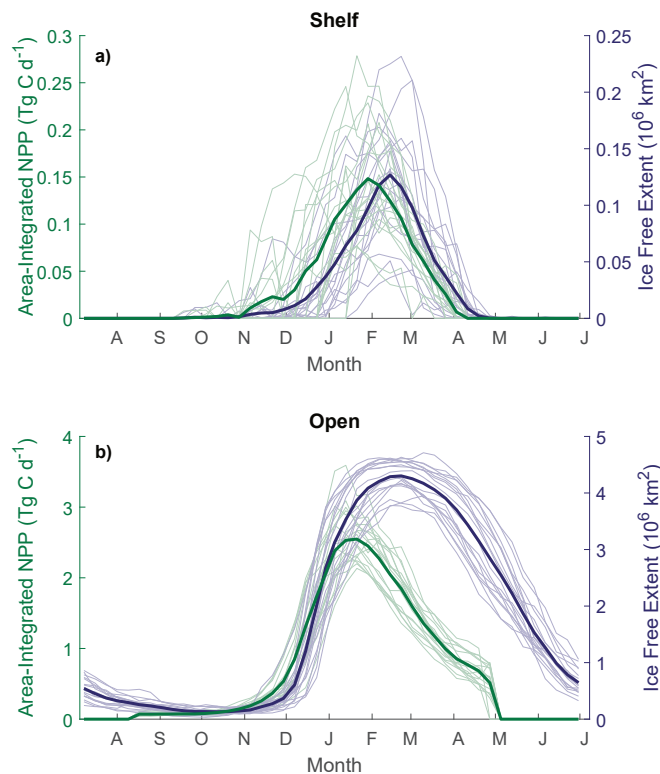


**Figure 4.** Seasonal cycles of total ~~time-integrated-area-integrated gap-filled~~ NPP (green) and ice-free ~~Extent extent~~ (blue) across the (a) ~~open ocean-shelf region~~ and (b) ~~shelf-region open ocean~~. Bold lines represent the 18-year mean, and thin lines show the annual variability.

### 3.2 Inter-annual variability and trends

No secular trends in total annual NPP were observed in the Weddell Gyre or the open-ocean region. Inter-annual variability is large, with production over the austral year in 2006 reaching 220 Tg C, while only 111 Tg C in 2015 (Fig.3.Bc). Successive

295 NPP minima in 2008 and 2014-2015 may indicate a cyclical pattern with a period of 6-7 years, but a longer timeseries is needed to determine this conclusively. Likewise, no secular trend was observed in any of the sea-ice variables within the Weddell Gyre or open ocean over the study period. Potential causes of variability are multiple, including ice-free area, ice-free days, timing of ice retreat, cloudiness, wind speed and direction, sea surface temperature, vertical nutrient supply, glacial contribution. We investigate a number of these in the discussion below.

300 In contrast, ~~trends in NPP and sea-ice are a trend in NPP is~~ seen in the shelf region. ~~Total annual NPP on the shelf has significantly declined during the study period~~ In the CAFE model, imputed NPP declined by 3% per year,  $p=0.02$  (Fig. 3.b). A similar rate of decline, although less statistically significant, is seen in the other NPP models. The directly-observed CAFE estimates of NPP decreased more rapidly (average decrease of 57% per year,  $p<0.01$ ). As with total NPP,  $p=0.001$ ), underscoring the large influence of missing NPP data in the annual summer maximum IFA has decreased across the shelf  
305 ~~region by 1.3% per year on average. However, these trends.~~ Westberry et al. (2023) describe other potential causes for trends seen in NPP products (e.g. physiological changes in phytoplankton and decoupling of Chl-a and NPP), and emphasise the difficulty in identifying trends in NPP data and inferring drivers of trends. The trends seen here are sensitive to the occurrence of extremes in the early part of the time-period when there were polynyas was a collapse of the Larsen B ice shelf along the Antarctic Peninsula (Peck et al., 2010). No trend is seen in the shelf NPP nor IFA when these first 3 years are  
310 ~~removed from analysis when the first data point (year 2003) is removed.~~

Pearson correlation tests were carried out to determine the correlation between NPP and IFA. Single and multiple linear regressions were then performed to assess the individual and combined effects of ~~time and~~ open water area and time (year as well as duration of ice-free season visible to the satellite) on total annual NPP. Summer maximum IFA represents the largest area that is available for NPP to occur in a year. Furthermore, because the winter sea-ice edge in the Atlantic sector largely  
315 extends beyond the Weddell Gyre boundaries used in this current study region (Fig. 1), the maximum IFA (minimum SIA) is also an indicator of the total area of SI retreat ~~in~~ across the region within a year. The winter maximum sea-ice area within the study region box is much less variable than the summer maximum ice-free area (standard deviation:  $6.6 \times 10^4$  and  $2.3 \times 10^5$  km for the winter SIA and summer IFA respectively). The study area is almost entirely ice-covered each winter, and any variability in the actual maximum sea-ice extent occurs north of the study region and is not significantly reflected in the  
320 study box. Regression analysis shows a significant relationship between the annual maximum IFA and total NPP (but that only explains approximately half of the variance), indicating that years with greater IFA result in more total NPP (Fig. 5). This relationship is seen in both the raw and imputed NPP estimates, but imputed NPP is shown in Fig. 5 and discussed here. IFA-NPP regressions for all NPP models can be found in Appendix Fig. A3. In the Weddell Gyre, 62% and open ocean sub-region, 42% of the inter-annual variability in total annual NPP can be explained by variability in the summer maximum  
325 IFA. Within the sub-regions, this relationship was strongest in the open ocean region, with 55% of the variance in total annual NPP explained by the summer maximum IFA (in each region ( $p=0.002$ , Fig. 5). In a and b). This relationship was strongest in the shelf region, 40% with 55% of the variability in total NPP is being explained by the yearly maximum IFA. As with the timeseries trends, the first three years had a large influence on the fitted regression model for the shelf region, as indicated by



high Cook's Distance values. The effect of the annual maximum IFA on NPP within the shelf region was weakened when the first three years were removed from the regression ( $R^2=0.34$ , over the shelf ( $p=0.01$ )).

In the open ocean, and in the Weddell Gyre as a whole, the area-normalised annual mean NPP for each region is not correlated with any sea-ice variables. However, the shelf region sees positive correlations between area-normalised annual mean NPP and mean IFA ( $R^2=0.66$ ;  $p=0.002$ ), sea-ice retreat ( $R^2=0.58$ ;  $p=0.011$ ), and mean visible days ( $R^2=0.76$ ;  $p<<0.001$ ). This correlation indicates that NPP in the shelf region is more intense when there is greater IFA. It is plausible that this correlation arises from the spatial dependence of NPP intensity in the shelf region, *i.e.* more IFA consistently indicates that a region with particularly intense production has been exposed, Fig. 5.c). Note that our annual NPP estimates are not independent of IFA, due both to NPP being set to zero under ice and to the IFA adjustment involved in gap filling. Therefore, the strength and statistical significance of these relationships are unsurprising and should be interpreted with caution. We therefore focus interpretation in the discussion on information contained in the residuals, with the unexplained variability being just as important.

Across the Weddell Gyre, and throughout the measurement period, a wide range of "satellite-visible days" were recorded. The mean number of satellite-visible days (days where the surface ocean is both ice-free and visible to MODIS-Aqua before the solar angle restricts satellite observations) across the open ocean was 92-94 days, but due to the size of the region and the rate of sea-ice retreat, there was a large range in the number of satellite-visible days seen at any given satellite pixel across the open ocean in any given year (0-260-262). The mean duration that the shelf region was visible to ocean-colour satellites was 35-49 days (range of 0-135-0-133 days for individual satellite pixels in individual years). Thus, on a pixel-by-pixel basis, we can use this pixel-scale variability to further assess the relationship between ice cover (visible days) and NPP. The annual area-normalised annual NPP in any location (pixel) is significantly correlated to the length of time it is visible to the ocean-colour satellite during the year. Fig.6 shows that, in general, locations that are visible to the ocean-colour satellite report greater annual NPP than locations which were visible for fewer days an initial steady increase in in annual NPP with increasing satellite visible days in both the open ocean and on the shelf. However, in the open ocean, the rate of increase slows beyond ~120-130 ice-free days (when the linear and asymptotic lines cross/diverge). In the shelf region, the increase in NPP when visible for longer is greater than in the open ocean (one-tailed t-test (34 df) = -6.195,  $p<0.005$ ), suggesting a more rapid response to earlier ice melt/longer ice-free (satellite-visible) periods. However, it is notable that in the density distribution, the majority of the pixels are only observable for very short periods, and importantly, seldom longer than 100 days. CAFE NPP on the shelf does not show signs of tapering off with increasing satellite-visible days. However, this is difficult to confirm, as very few on-shelf pixels are visible to the CAFE model for >130 days. Notably, other NPP products show similar relationships between visible days and NPP (Appendix Figures A4, A5, A6).

### 3.3 Aligning satellite and subsurface perspectives

Satellite observations indicate that, in the open ocean, the strong positive correlation between visible days and NPP degrades after around 120-130 visible days, indicating that other processes (e.g. grazing, nutrient availability) potentially begin to limit NPP after this much exposure. To complement and deepen this analysis, waters have been ice-free for more than 4 months. However, as described in Section 2.4, the ocean-color satellite loses coverage in late summer, when the solar angle decreases

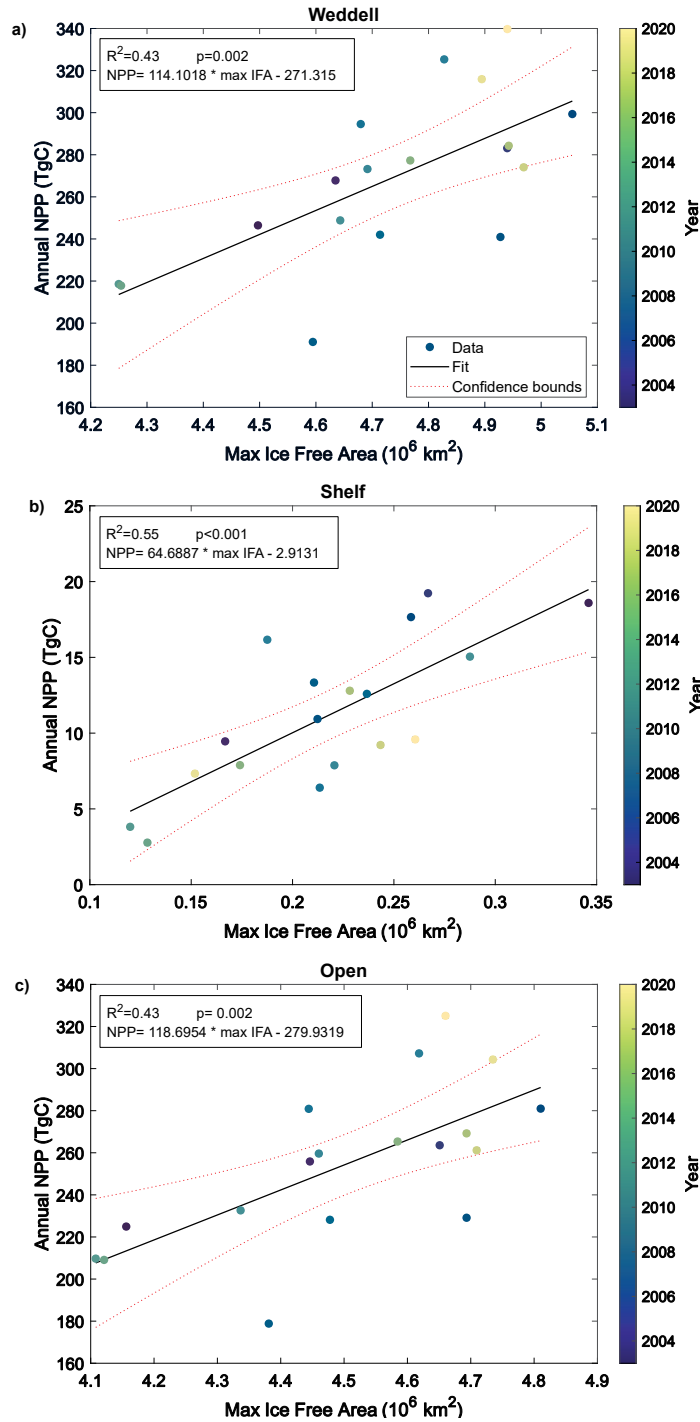


**Figure 5.** Relationship between annual maximum ice-free area and permuted annual NPP :-The variability in within a) the maximum area of ice-free water each year explains entire study region; b) the inter-annual variability in total NPP across the Weddell Gyre shelf region and each of c) the subregions open ocean region. Dotted lines represent the 95% confidence bounds.

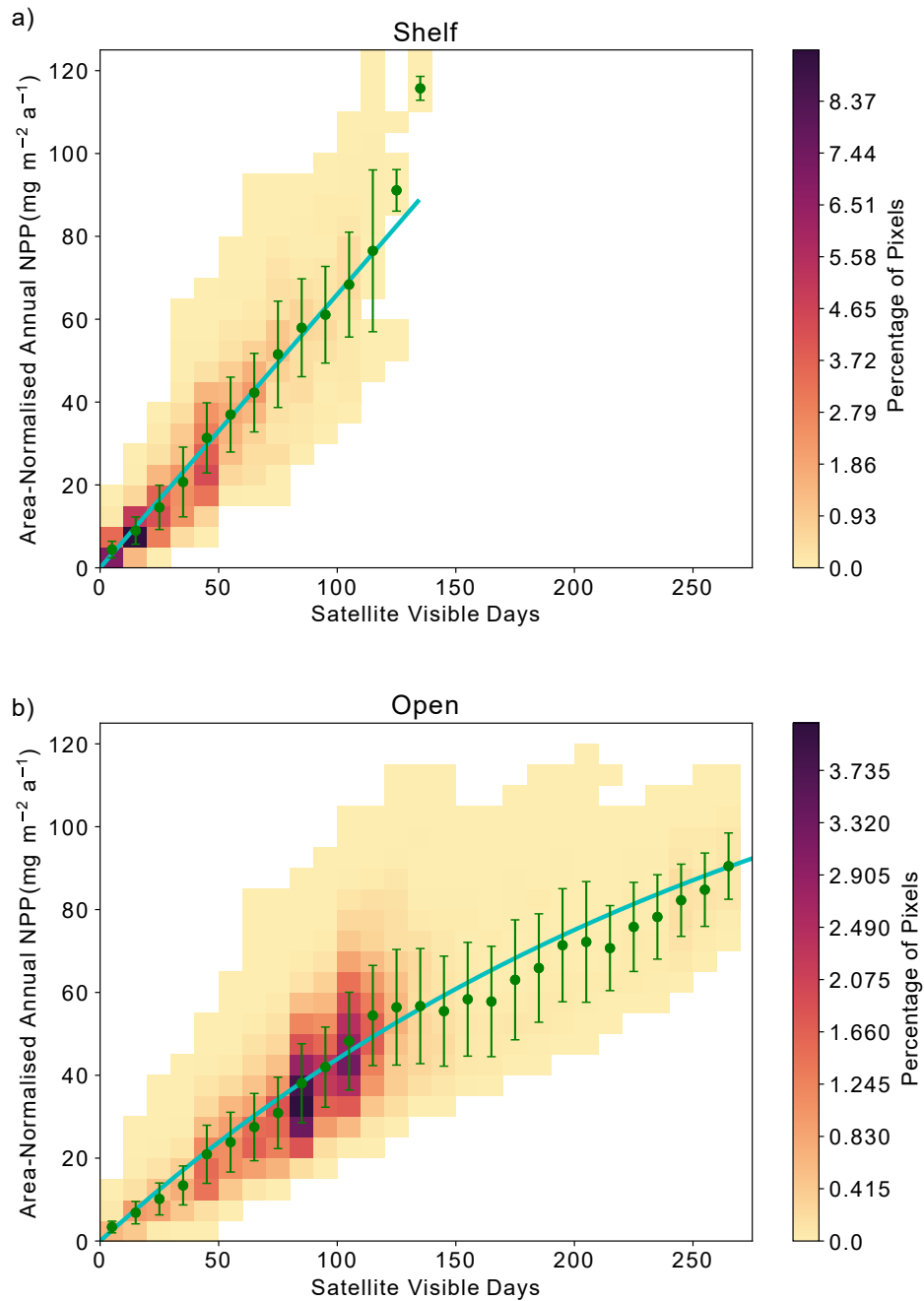


**Figure 6.** Relationship between area-normalised annual NPP and number of visible days (VD) for all satellite data pixels over the timeseries. Heatmap shows the area-normalised density distribution of data points, while the lines show the (a) non-linear-linear (open-oceanshelf;  $NPP = 0.66 * VD$ ) and (b) linear-non-linear (shelfopen ocean;  $NPP = 151.12 \times (1 - e^{-VD \frac{0.52}{151.12}})$ ) relationships for the whole timeseries. VD bin means  $\pm$  standard deviation are plotted in green.

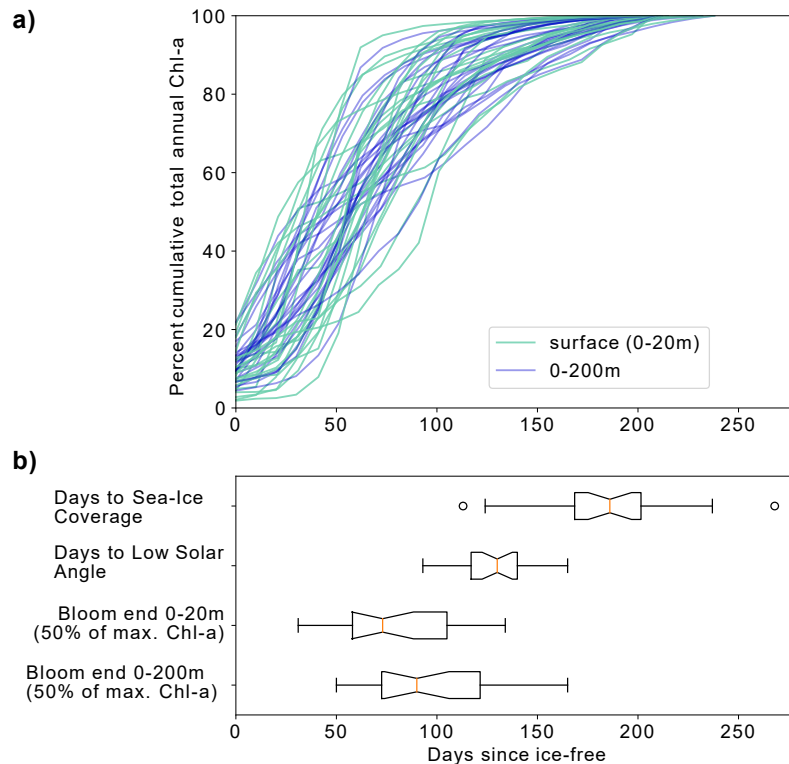


**Figure 7.** a) Percent cumulative Chlorophyll-a in the surface (0-20m) and between 0-200m for all completed annual cycles by the floats between 2015-2021. **Upper-panel indicates b) Box and whisker plots** indicating the range in the number of days from ice melt to (i) sea-ice return, (ii) low solar angle (loss of satellite observations), (iii) surface bloom end and (iv) depth-integrated bloom end. **Orange line represents the median value for each, the box represents the first and third quartiles, while the whiskers extend to 1.5 times the inter-quartile range.**

below 20°. As a result, it is uncertain whether further NPP is occurring, and therefore, missed after this point. Assessment of float Chl-a and POC (as proxies for phytoplankton growth/biomass) can reduce this uncertainty by indicating whether phytoplankton are still present in the surface ocean and/or whether growth may still be occurring beyond the date when satellites lose visual coverage. Therefore we seek to address **the same question** if significant growth is missed after loss of satellite coverage in late summer and whether the same relationship between ice-free days and phytoplankton growth is seen in the available float observations. Although these data come from drifting platforms, rather than fixed points, we can enquire how the seasonal **eyele-cycles** of Chl-a **unfolds-and POC unfold** in each year, and specifically how **it evolves they evolve** relative to light availability. It is worth noting that **,due to the depth-restrictions of floats,** these data all represent open ocean conditions **as floats are not deployed in regions shallower than 2000m.**

Figure 7.a shows the progression of the bloom ~~for (Chl-a as proxy for growth)~~ for each year for each float, starting at the first ice-free day (~~bottom panel~~). On average, 10% of the integrated annual Chl-a is recorded under the sea ice (max. 23%), so the majority of Chl-a is observed after the floats are considered to be in ice-free conditions. We evaluate the bloom progression for both the surface (0 to 20m; analogous to satellite-observed depths; ~~green lines in Fig.7.b~~) and upper 200m (~~blue lines in Fig.7.b~~), and define the bloom end as the date that Chl-a concentrations declined and remained below 50% of their seasonal maximum. Across all years and floats, median surface bloom end occurred ~~85-73~~ days after ice melt (range ~~41-144-31-134~~ days), while median depth-integrated bloom ended on day ~~96-90~~ following ice melt (range ~~50-155-50-165~~ days; Fig. 7; ~~upper panel.a~~). The later date of bloom end for the depth-integrated values indicates that ~~, on average, primary production primary production could be continuing~~ in the water column ~~continued~~ at depth until ~~slightly~~ later in the season ~~-than at the surface~~. Certain float years in Figure A2 (panels a-d and k) see a concurrent increase in Chl-a and POC in the depth integrals that indicates that active production/growth is taking place, as opposed to changes in phytoplankton physiology or community composition driving changes in Chl-a (Thomalla et al., 2017).

A significant decline ~~of the bloom consistently occurred~~ in Chl-a consistently occurred prior to the low solar angle and substantially before the return of ice coverage (Fig. 7; ~~upper panel.b~~). Overall, surface bloom ends preceded low solar angle by median 50 days (range: 100 days before to 10 days after) and preceded ice coverage by median 130 days (range: 176 days before to 0 days). Surface and depth-integrated blooms ended before the date of low solar angle and the date of sea-ice return in all but one of the 23 float-years. This ~~supports the supposition inferred from the satellite data that , in regions experiencing an extended period of ice-free days, NPP becomes limited by~~ result adds independent support to the satellite-derived finding that open Weddell Gyre phytoplankton blooms decline after 3-4 months ice free and extends the finding to full euphotic zone. The slightly later decline in depth-integrated Chl-a relative to surface Chl-a also suggest that factors other than light contribute to the end of the bloom.

## 4 Discussion

### 4.1 Biological carbon uptake in the Weddell Gyre dominated by NPP in open ocean region

This study shows that over the last 18 years, open ocean productivity has a dominant role in the ~~biological~~ carbon cycle of the Weddell Gyre, in agreement with synoptic ship-based studies (MacGilchrist et al., 2019; Brown et al., 2015). MacGilchrist et al. (2019) documented that the region was a net annual CO<sub>2</sub> sink only due to a large amount of carbon sourced from biological activity in the central ~~gyre~~ Weddell Gyre accumulating in the local Circumpolar Deep Water; horizontal circulation of this water mass out of the Weddell Gyre then facilitates sequestration of carbon over ~~long-climate-relevant (centennial to~~ ~~millennial)~~ time scales.

~~Nevertheless, many studies of Weddell Gyre productivity have focused on the shelf and coastal regions surrounding Antarctica because of the high local rates of NPP and the importance of deep-water formation for carbon export (Arrigo et al., 2008a, 2015; Yager et al. While we find similarly high rates of coastal NPP, we additionally show that the SIZ beyond coastal areas also exhibits considerable biological carbon uptake. This is in agreement with Arrigo et al. (2008b), who found that rates of productivity in~~

405 ~~the recently uncovered waters of the marginal ice zone can be as high as polynyas and shelf systems. They also identified the Weddell Sea marginal ice zone as the largest and most productive marginal ice zone of all the geographic sectors investigated (25% greater than the Ross Sea marginal ice zone; Arrigo et al., 2008b), emphasising the importance of this region to the SO biological carbon pump.~~

Our current study highlights the importance of the Weddell Gyre's open ocean compared to the shelf region, showing that  
410 the majority (~~99~~93-96%) of the carbon uptake by phytoplankton in the Weddell Gyre occurs there, despite higher daily rates of NPP observed on the shelf. This is due to its far greater areal extent (an order of magnitude larger than the shelf region) and much longer ice-free growing season. In light of our results here, we highlight the need for future research in this region to further quantify the contribution of open ocean production to the biological carbon pump. Satellite NPP values are often underestimated due to the negative biases in spatial coverage within NPP products. Gap-filled, permuted NPP estimates were  
415 calculated to reduce these uncertainties and biases, particularly in the shelf region where spatial coverage was impacted by significant gaps in the data. These values are considered to be more realistic estimates of the total NPP occurring in the two regions. It is important to note that the gap-filling correction assumes that mean NPP is equal in the visible and non visible portions of the region and so could therefore still carry uncertainties.

## 4.2 Drivers of NPP variability

420 Our results show a clear relationship between ~~sea-ice~~sea ice and NPP on an inter-annual timescale (Fig. 6), but that explains only 40-55% of the variance in NPP. A large fraction of this ~~likely~~ arises from the role of sea-ice cover in setting light availability in the SIZ. We discuss the nature of this relationship (~~which accounts for 40-55% of the variance in NPP~~) in the following section, before exploring other possible sources of ~~interannual~~inter-annual variability.

### 4.2.1 ~~Sea-ice~~Sea ice as a control of light availability

425 Light availability is restricted under ~~sea-ice~~sea ice, so when ~~sea-ice~~sea ice retreats, light limitation caused by sea-ice coverage is alleviated (Twelves et al., 2021; Arrigo and Van Dijken, 2011; Arrigo et al., 2015; Rohr et al., 2017; Smith and Comiso, 2008). Therefore, while the annual NPP cycle at high latitudes is generally driven by regular seasonal changes in solar angle/position through the year (Ardyna et al., 2017; Arrigo et al., 2008b; Park et al., 2017; Smith and Comiso, 2008), within the SIZ, the initiation of growth and the total NPP that results is also mediated by sea-ice cover and its inter-annual  
430 variability (Rohr et al., 2017; Twelves et al., 2021). ~~Satellite and float data presented here reflect this: in Fig. 4, where the increase in total NPP from late November mirrors the retreat of~~ Our basin-wide satellite-based NPP analysis assumes no NPP under ice and, as expected, finds sea-ice ~~(increase in the IFA); and in Figures 7, 2, A1, where float profiles show that the majority of growth occurs after floats become ice-free (in spite of Chl-a in the water column starting to increase while floats are still under ice).~~ In an aggregated sense, our basin-scale analysis of the Weddell Gyre confirms that the variability  
435 in the sea-ice coverage over the timeseries is to be a dominant driver of ~~the~~ inter-annual variability in NPP: ~~annual~~. Annual summer minimum SIA (summer maximum IFA) in particular explains 40-55% of the NPP variability within the subregions and ~~60% of NPP variance in~~ the Weddell Gyre overall (Fig. 5). ~~This finding is consistent with the suggestion that larger~~



~~areas of~~ The float data showing that 2-23% of integrated Chl-a (and 7-30% of surface POC; Table. 1) is present potentially before sea-ice retreat suggests that our the satellite analysis may over-estimate somewhat the correlation between IFA and NPP. Recent studies (Bisson and Cael, 2021; Hague and Vichi, 2021; McClish and Bushinsky, 2023) have also reported the presence of considerable amounts of Chl-a under sea ice as well as highlighting the onset of growth prior to complete sea-ice retreat (Hague and Vichi, 2021; McClish and Bushinsky, 2023). However, while our float observations also indicate that biomass tends to increase before complete ice retreat, our results still clearly show IFA as a major productivity driver. Strong phytoplankton growth follows ice melt (Fig. 7) and the majority of phytoplankton biomass is found in ice-free water provide more space for NPP to take place (Arrigo et al., 2008b, 2015) conditions (Figs. 2, A1 and Table 1). Similarly, in McClish and Bushinsky (2023), the break-up of sea ice initiates the increase in Chl-a and POC, highlighting the light limiting control of sea ice on phytoplankton growth. Recent work has shown that seasonal to inter-annual variability in Antarctic sea-ice cover exhibits substantial predictability (Libera et al., 2022; Bushuk et al., 2021). The strong relationship seen here between sea ice and NPP therefore indicates that sea-ice predictability may translate into predictability of NPP, with consequences for fisheries and ecosystem management. Indeed, this link between sea-ice and NPP predictability was recently shown in a perfect model context (Buchovecky et al., 2023).

Despite this strong control of IFA on total NPP, there is still a considerable amount of inter-annual variability that is not explained by the variability in the summer maximum IFA (Fig. 5). Some of the unexplained variance in NPP could be related to the spatial pattern patterns and variability of sea-ice retreat. Daily average NPP exhibits substantial spatial variations (not shown), with “hot-spots” hotspots in the eastern Weddell Gyre, particularly around Maud Rise, along the narrow shelf in the east, and in the open ocean near the eastern boundary of the Weddell Gyre. These hotspots are thought to be set by comparatively high levels of nutrient supply (e.g. Vernet et al., 2019; Geibert et al., 2010; Arrigo et al., 2015) (e.g. Vernet et al., 2019; Geibert et al., 2010; Arrigo et al., 2015; Moreau et al., 2023). Consequently, in any given year, spatial variations in where and when sea-ice sea ice retreats will determine whether or not these hot spot regions are exposed and for how long, with concomitant impacts on integrated carbon uptake across the Weddell Gyre.

Inter-annual variability in sea-ice cover is set by physical mechanisms, such as atmospheric forcing (e.g. phase of the Southern Annular Mode) and ocean forcing (e.g. sea surface temperature) (Kumar et al., 2021). Recent work has shown that seasonal to inter-annual variability in Antarctic sea-ice cover exhibits substantial predictability (Libera et al., 2022; Bushuk et al., 2021) - The strong relationship seen here between sea-ice and NPP therefore indicates that sea-ice predictability may translate into predictability of NPP, with consequences for fisheries and ecosystem management. Indeed, this link between sea-ice and NPP predictability was recently shown in a perfect model context (?) Moreau et al. (2023) found that strong winds transport sea ice towards the shelf, potentially removing light limitation to the surface waters as a result.

At a local level, area-normalised NPP appears strongly related to the duration that an area has sufficient available light for satellite detection (Fig. 6; see Sect. 2.4 for a discussion on the distinction between visible days and light availability). Over shelf sea regions, sea-ice persists for longer and reforms re-forms earlier than in the open ocean, meaning that the duration of light availability is set by both the retreat and return of sea-ice sea ice (Fig. 4). The strongly linear relationship in Fig. 6.a suggests that phytoplankton on the shelf are primarily limited by light availability, itself controlled by sea-ice cover. This is

consistent with the expectation that the shelf sea regions are nutrient (specifically iron) replete (Arrigo et al., 2015; Boyd et al., 2012; McGillicuddy et al., 2015; Sedwick and Ditullio, 1997), such that they do not become nutrient limited during the short  
475 ice-free season.

#### 4.2.2 Nutrient limitation

In the open ocean ~~the~~ subregion, once the sea ice is gone, other factors beyond light limitation – such as nutrient supply – determine how much NPP takes place, and for how long (Fig. 6.b). We hypothesise that the open ocean experiences a progression from light limitation when sea ice is present to nutrient limitation once the ice-free season has persisted longer  
480 than ~80-130 days (Figures 6.b,7). This picture is consistent with other studies that identify a progression of limiting factors in the SO (Arrigo et al., 2015; Ryan-Keogh et al., 2017; Sedwick et al., 2011; Twelves et al., 2021; von Berg et al., 2020). In the open ocean, the earlier melt and later return of sea-ice sea ice compared to the shelf region (Fig. 4) means that the number of visible days (and by consequence ice-free season) can be much longer-greater (Fig. 6). Consequently, we can see a tapering-b).  
The weakening/plateau of the relationship to-between the number of visible days and NPP (Fig. 6) indicating that other factors  
485 in the open ocean.b) indicates the exertion of a limiting control, such as nutrient availability or top-down controls, mediate mediating NPP towards the end of the growing season, and thus impact its interannual variability.

The sub-surface float data further support the finding that factors other than light impact NPP towards the end of the growing season in the open ocean. support this finding: For the majority of float years, a decline in Chl-a occurs before light limitation returns (Fig. 7) – i.e. before the solar angle is below critical ( $20^\circ$ ) in March, and well in advance of the return of sea-ice sea ice  
490 ice to the float's location (Fig. 7). The average timing of this decline (73 days at the surface) is broadly consistent with what is seen in the satellite results. The implication is that the decline in growth after 2-3 months of ice-free conditions leads to a suppression in annually integrated NPP in areas where the ice-free season lasts longer than approximately 3-4 months.

#### 4.2.3 **Iron**

~~In the open ocean subregion, once the sea-ice is gone, other factors – such as nutrient supply – determine how much NPP takes  
495 place, and for how long (Fig. 6). We hypothesise that the open ocean experiences a progression from light limitation when sea-ice is present, to nutrient limitation once the ice-free season has persisted longer than 80-120 days (Figures 6,7). This picture is consistent with other studies that identify a progression of limiting factors in the SO (Arrigo et al., 2015; Ryan-Keogh et al., 2017); Thus, nutrient limitation could be setting an upper limit to NPP and effectively dampen the influence of sea-ice on interannual sea ice on inter-annual variability, particularly in areas that experience longer ice-free seasons.~~

500 The ~~hypothesis that nutrient limitation is the factor controlling NPP in areas of long ice-free seasons is~~ nutrient limitation hypothesis is well supported by existing literature. Much of the SO is macro-nutrient replete but micronutrient-micro-nutrient limited (primarily by iron (de Baar et al., 1995; Hauck et al., 2015) and possibly by manganese (Hawco et al., 2022)). Some areas of the SO also experience silicate limitation after the spring bloom (Lafond et al., 2020; Quéguiner, 2013), although this is unlikely in the Weddell Gyre, as high concentrations of silicate have been documented through extensive repeat sections  
505 through the region (Hoppema et al., 2015). Iron limitation has been found to be more prevalent with distance from the ice

shelf, as well as later in the growing season, when the ‘winter inventory’ has been utilised (Twelves et al., 2021; Boyd et al., 2012; Hoppema et al., 2007). In the Weddell Gyre, the areas that have the longest ice-free/satellite-visible seasons are also generally the areas furthest from the ice shelf and continent, and therefore furthest from an abundant iron supply. We postulate therefore that iron limitation ~~is~~ could be a major driver of the slowing/decline in NPP that occurs prior to sea-ice return in the open ocean (Figures 4, and 6).

Our hypothesis of iron limitation at the end of the growing season is supported by the sub-surface Chl-a ~~data and POC~~ observed by floats (Appendix Figure A1). ~~In particular, the continuation~~ Figures A1 and A2). Changes in Chl-a concentrations can arise from several situations aside from growth/accumulation of biomass: photo-acclimation, nutrient limitation and changes in phytoplankton community composition (Thomalla et al., 2017). Comparing Chl-a to POC, we can assess what may be causing changes in Chl-a. The presence of elevated Chl-a ~~close to concentrations close to or below~~ the base of the mixed layer (~~Appendix Figure A1, often (but not always)~~) after the cessation of the initial surface bloom ~~indicates~~ (Appendix Figure A1), suggests that phytoplankton are benefiting from replenishment of nutrients from below the mixed layer through diapycnal mixing (Arrigo et al., 2015; Taylor et al., 2013). ~~Float data suggest that deeper blooms are different in type/composition to those occurring at the surface due to differing persistence (Appendix Figures 2, A1). This further supports the hypothesis that nutrient limitation is playing a major role in phytoplankton growth, although~~ Elevated POC signals coincide with increased Chl-a in the majority of these cases, providing evidence that active production is taking place at depth (Appendix Fig. A2). Surface nutrient concentrations are thus likely to be limiting phytoplankton growth in many areas of the ice-free Weddell gyre, although float data do not allow us to quantify its net impact on NPP cannot be confirmed. Grazing pressures may also be important in driving the differences in surface and sub-surface phytoplankton dynamics (Baldry et al., 2020, also see Section 4.2.3).

The complexity of the relationship between light and nutrient limitations – and their implications for ~~interannual~~ inter-annual variability in annual NPP – is ~~exemplified~~ highlighted by the occasional occurrence of a secondary (temporally separated) late-summer bloom (Appendix Figure A1. e.g. ~~floats panels a~~ floats panels a) 5904397: 2018, 2019; ~~b~~ b) 5904467: 2018; ~~c~~ c) 5904468: 2018, 2019; ~~d~~ d) 5904471: 2018). ~~These~~; ~~g~~ g) 5905992 2020). As seen in the matching Chl-a and POC signals at depth, the second peaks in surface and depth integrated Chl-a that suggests a late-summer bloom are matched by simultaneous POC increases at these times, implying active growth within the phytoplankton community (Appendix Fig. A2). There are four float years (Appendix Fig. A2 h) 5905994: 2020; j) 5906033: 2020; and k) 5906034: 2020, 2021) that saw small increases in Chl-a at the end of the ice-free season without a concurrent increase in POC. We conclude that the increase in Chl-a in these cases may be a result of phytoplankton photo-acclimating to the decreasing light conditions. The secondary blooms typically follow a set pattern (von Berg et al., 2020): when sea-ice melt occurs earlier, iron resources are then also depleted earlier in the growing season.

The secondary bloom initiates when micro-nutrients are replenished from entrainment/diapycnal mixing (Arrigo et al., 2015; Taylor et al., 2013), before it is later cut off by a combination of sea-ice return and reduction in PAR due to a shoaling of the light penetration depth (Appendix Figure A1). Two temporally separate blooms are not always visible, with previous studies suggesting that the timing of the first bloom may be a key driver for this (von Berg et al., 2020), otherwise the two blooms will overlap in time sufficiently as to be indistinguishable. Further iron limitation, grazing pressure, or low light levels bring an end to the second bloom. The observation of double blooms, particularly with the latter sometimes occurring at different locations

in the water column, indicates that the processes limiting NPP or acting as a brake on its magnitude are not identical in all locations/water depths.

As with sea-ice cover and its impact on light limitation (Sect. 4.2.1), physical mechanisms drive inter-annual variability in nutrient supply, with plausible implications for the variability in total annual NPP. Changes in iron supply to the ocean surface and thus the alleviation of iron limitation can occur through variability in mixing (~~(?Biddle and Swart, 2020; Swart et al., 2020)~~ (Prend et al., 2022; Biddle and Swart, 2020; Swart et al., 2020), upwelling of iron rich deep waters (Moreau et al., 2023; Twelves et al., 2021; Hoppema et al., 2015; Vernet et al., 2019), as well as supply of icebergs to warmer areas of the gyre Eastern Weddell Gyre (~ 20 - 25 °E) (Geibert et al., 2010). Furthermore, in addition to its impact on light availability, sea-ice dynamics play an important role in supplying iron to the SIZ (Boyd et al., 2012), possibly complicating the impact of sea-ice variability on total annual NPP.

### 4.2.3 ~~Other factors limiting NPP~~ Grazing

Within the scope of this study, it has not been possible to assess additional controls on phytoplankton growth, beyond sea-ice-induced light availability (Sect. 4.2.1) and nutrients (Sect. 4.2.2). However, it is plausible that other factors could be important for the inter-annual variability of NPP, specifically top-down controls (such as zooplankton grazing or microbial activity). The presence of ~~sea-ice~~ sea ice can act to decouple grazers and phytoplankton (Hoppema et al., 2000; Rohr et al., 2017; Smetacek et al., 2004), and as micro-nutrient availability diminishes, grazing may increasingly contribute to the decline of the NPP bloom such that, by late summer, grazer populations may be ~~also exerting top-down control over NPP~~ the dominant control of phytoplankton biomass/communities (Rohr et al., 2017; Smetacek et al., 2004). Vernet et al. (2019) review various studies that have highlighted the abundance of higher trophic levels in areas of the Weddell Gyre, and Kauko et al. (2022) recently highlighted krill as exerting top-down (grazing) control on diatom populations in the Kong Håkon VII Hav. However, there is a lack of widespread zooplankton research that has taken place through the Weddell Gyre open ocean, and so it is difficult to determine whether grazers are a significant control of phytoplankton. Variability in ecosystem composition is also likely a significant contribution to the temporal and spatial signal of integrated NPP (Lin et al., 2021; Trimborn et al., 2019; Mascioni et al., 2021; Takao et al., 2020).

## 4.3 Implications for the future

Sea-ice extent around Antarctica is expected to change in response to anthropogenic global warming (Kumar et al., 2021; Ludescher et al., 2019; Casagrande et al., 2023). With its strong link to NPP, as exhibited in this study, changes in sea-ice dynamics could strongly impact biological carbon uptake in the Weddell Gyre. In turn, this could affect the ecosystem health as well as the contribution that the Weddell Gyre makes to global carbon uptake and climate (Henley et al., 2020).

Our results strongly suggest that, within the SIZ, a larger ice-free area and longer ice-free season (such as might be expected in a warmer world) will lead to higher total annual NPP in many regions, assuming there are no changes to other environmental variables such as nutrient supply and grazing. However, our results also indicate that this increase is not likely to be linear, and beyond a threshold in the length of the ice-free season, NPP will cease to increase at the same rate. ~~Furthermore,~~

by analogy to the permanently open ocean regions in the present-day Southern Ocean (Arrigo et al., 2008b), a region that becomes permanently ice-free in Our results further imply that nutrient supply is a key control on this upper limit for NPP in the present day in the open ocean. Consequently, how NPP will change across the Weddell Gyre may be expected to become comparatively unproductive. The implication is that while biological carbon uptake might initially increase in an increasingly becomes sensitive to how iron supply will change in the future. Such changes could also be mediated by changes in sea-ice dynamics due to their impact on stratification, mixing and upwelling (Moreau et al., 2023; Hoppema et al., 2015). In future warming conditions, increased stratification, combined with freshening from melting ice could act to cut off biological productivity by reducing the vertical nutrient supply (Bronsele et al., 2020). This will be particularly apparent in the open ocean, given its greater distance from terrestrial micro-nutrient sources. Noh et al. (2023) recently showed that, within CMIP models, Chl-a in the Arctic declines as a result of reduced nutrient supply when regions become ice-free Weddell Gyre, it is more than likely that this increase will have an upper limit, with the potential that NPP could decline in the long-term should the region become part of the permanently open ocean zone (Arrigo et al., 2008b).

Our results further indicate that nutrient supply is a key control on this upper limit for NPP in the present day, particularly in the open ocean. An. Despite being based in the Arctic, and thus differing physically and ecologically from the SO, this result in Noh et al. (2023) could point to a less productive Weddell Gyre in the future, should any of it become permanently ice-free. Notwithstanding changes in nutrient supply, an increasingly ice-free Weddell Gyre will see a greater expanse experiencing nutrient limitation late in the growing season. It is unclear whether the same limitations will have a similar effect on NPP in the shelf region should it become increasingly ice-free for longer than is currently seen (~ 130 days). Consequently, how NPP will change across the Weddell Gyre becomes sensitive to how iron supply will change in the future. Such changes could also be mediated by changes in sea-ice dynamics due to their impact on stratification, mixing and upwelling (Moreau et al., 2023; Hoppema et al., 2015).

## 595 5 Conclusions

This study used a complement of satellite and satellite-derived sea ice and NPP products as well as BGC-Argo float data observations of Chl-a and POC as proxies for phytoplankton biomass to assess the temporal and spatial variability in NPP and to characterise and quantify the relationship between NPP and sea-ice in the Weddell Gyre. It is clear that sea-ice dynamics are important in driving NPP in this region – both by initiating the seasonal pattern of growth and influencing the variability in annual NPP. Variability in the sea-ice coverage during 2003–2020 accounts for a high degree of the inter-annual variability in NPP, such that more sea-ice melt results in a greater basin-scale relationship between sea ice and phytoplankton growth. We find that sea ice is the primary control on Weddell Gyre NPP in areas that experience fewer than 70–130 ice-free area where light limitation is alleviated, thus producing a larger productive area for biological activity to take place in. Additionally, the longer an area is days per year. Beyond ~ 130 ice-free and visible to the satellites, days, float Chl-a and POC observations suggest that nutrients (likely iron) emerge as an important limit to growth, possibly co-limiting with top-down grazing control. We find that while the shelf region sustains higher instantaneous NPP during its ice-free window, the greater NPP occurs, although results

indicate that in the open ocean, NPP is limited before sustains 93-96% of the annual NPP of the Weddell Gyre, due to its larger area and longer ice-free season. Furthermore, while sea ice is a primary driver of inter-annual variability in total annual NPP in the Weddell Gyre, nearly half of NPP variability is still unexplained, motivating further study. We found no long-term trends in the Weddell Gyre sea-ice coverage resumes. Float data suggests that iron limitation may be the main control, but further research is needed to establish the limiting factors in the open ocean. Substantial spatial variability undoubtedly contributes to the variance in NPP, with consistent and sporadic hotspots of biological activity influencing this variability. Other non-sea-ice associated forcing mechanisms likely account for the remaining inter-annual NPP variability. Ultimately, future changes to extent or NPP during the study period. However, our results suggest that NPP will increase if sea-ice are expected to influence biological activity to a considerable extent. The open ocean of the Weddell Gyre has been shown to be more important than the shelf region in regards to the total NPP occurring each year due to its large spatial area and longer extent decreases in the future, at least until the Weddell Gyre is ice-free seasons. Consequently, future research should include studies of off-shore regions of the SIZ to further understanding on the drivers and limitations of SO NPP for longer than 130 days, at which point, controls other than sea ice may dominate. Finally, this work has highlighted the importance of using BGC-Argo float data to complement and corroborate satellite data analysis. The study highlights the need for development of quantitative float-based NPP measurements in the region, which would likely benefit from inclusion of PAR sensors on more floats.

*Data availability.* Raw data available from: Oregon State [www.science.oregonstate.edu/ocean.productivity/](http://www.science.oregonstate.edu/ocean.productivity/) and SOCCOM December 2021 Snapshot <https://doi.org/10.6075/J00R9PJW>

*Code and data availability.* Processed data from data sources above and code used to process data and create figures for this paper are available at <https://doi.org/10.5281/zenodo.7951184>

## Appendix A: Supporting Figures

~~Mean daily NPP. Green bars represent the shelf region value and blue bars for open ocean values.~~

*Author contributions.* Conceptualisation and design of study were carried out by all authors. Data preparation, analysis and writing by CCD. Editing was carried out by all authors

630 *Competing interests.* The authors declare no competing interests.



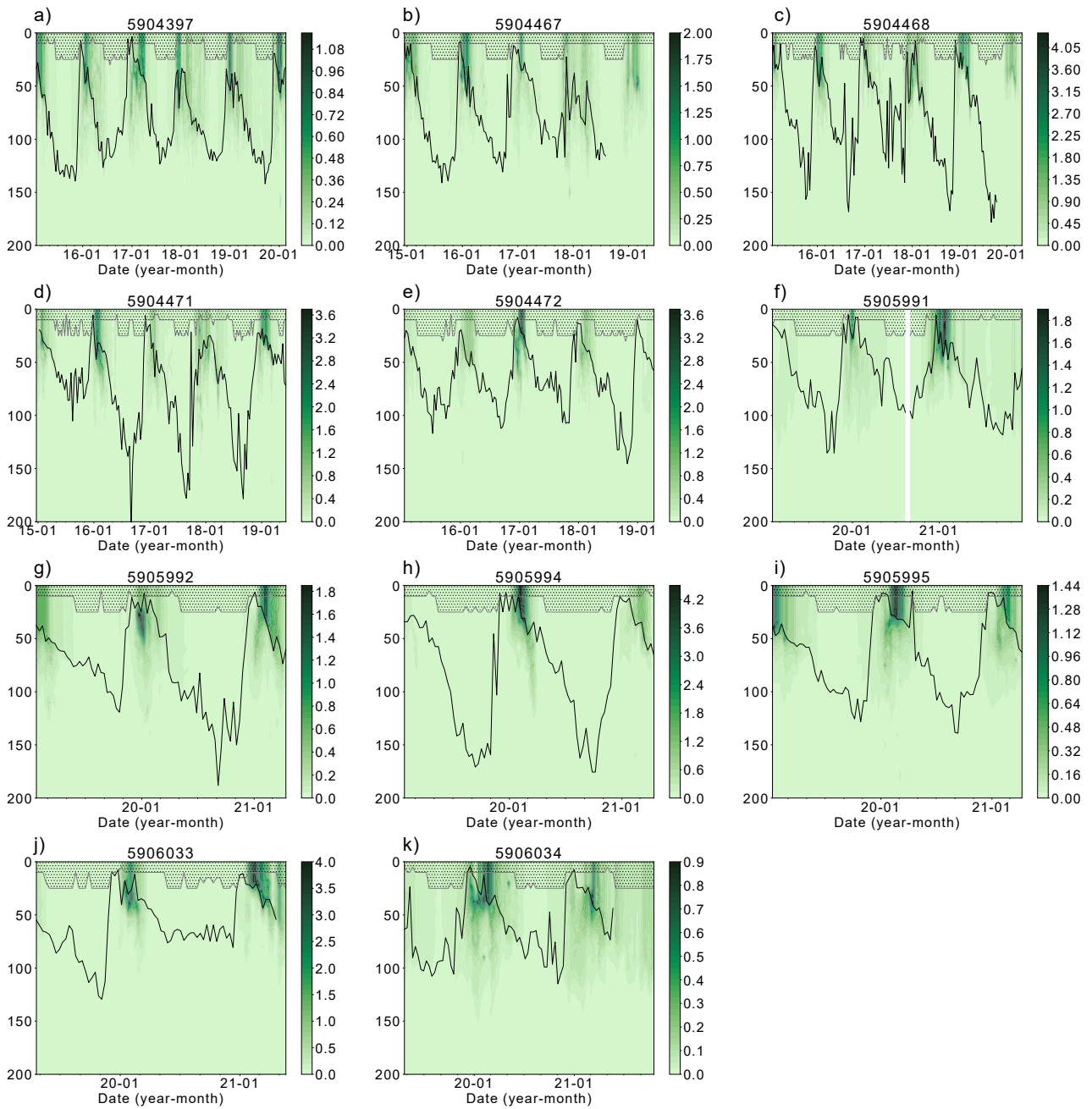


**Figure A1.** Chlorophyll-a concentration between 0-200m for each float found within the Weddell Gyre study region between 2014-2021. Black line represents the mixed layer depth and shaded areas represent the data extrapolated to the surface from the shallowest float measurement. Note colour scales vary between floats

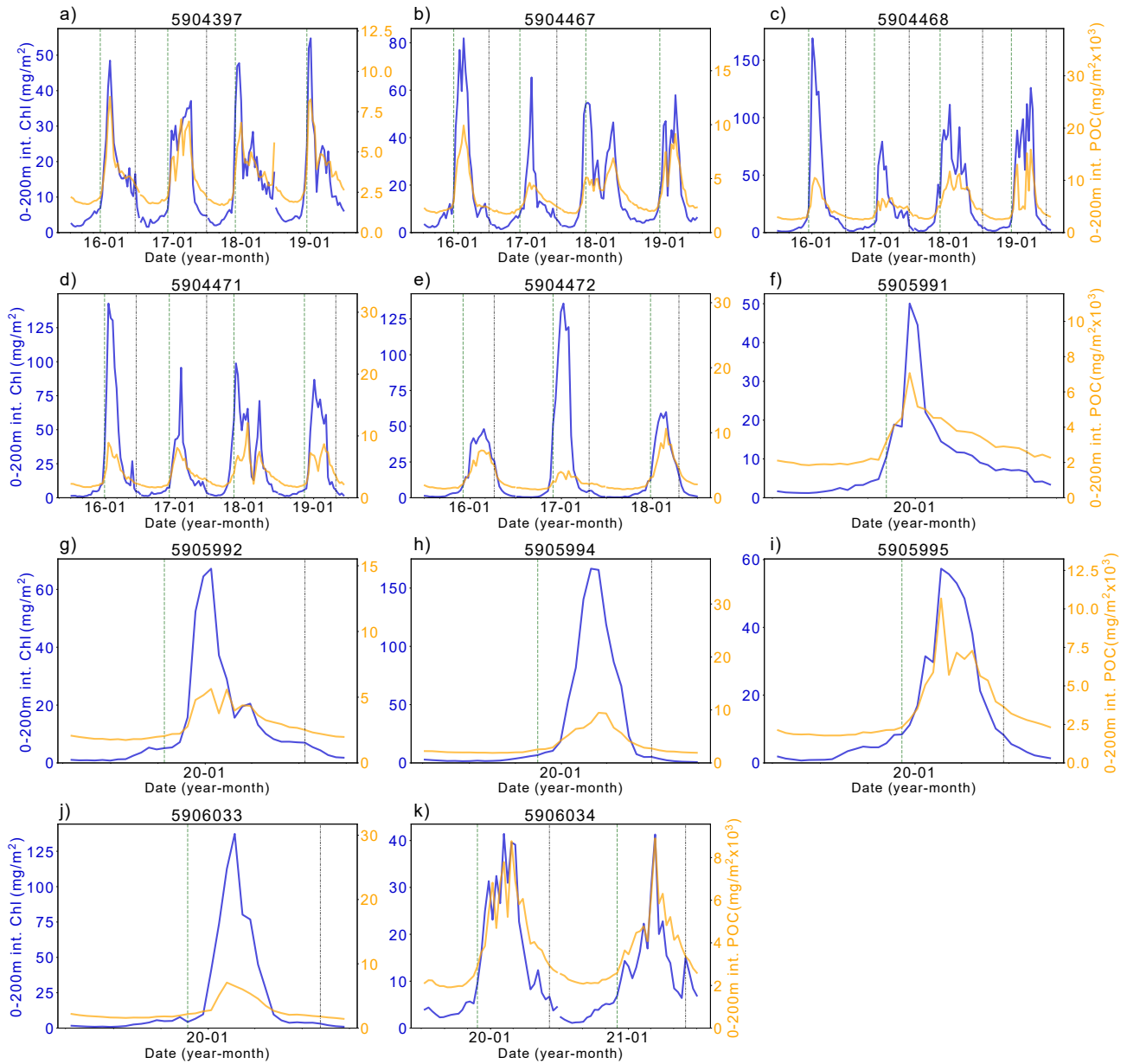


**Figure A2.** Satellite–float Chlorophyll-a (Chl-a) and particulate organic carbon (POC) comparison. Left y-axis mean Chl-a concentration values at (1) shows the closest pixel to location of float profile (orange line) and (2) integrated Chl-a between 0-20m-0-200m (light dark blue line). Right y-axis shows the integrated Chl-a POC between 0-200m (dark blue line). Vertical dashed green line indicates start of ice-free season; vertical dash dot blue line indicates start of ice-season.

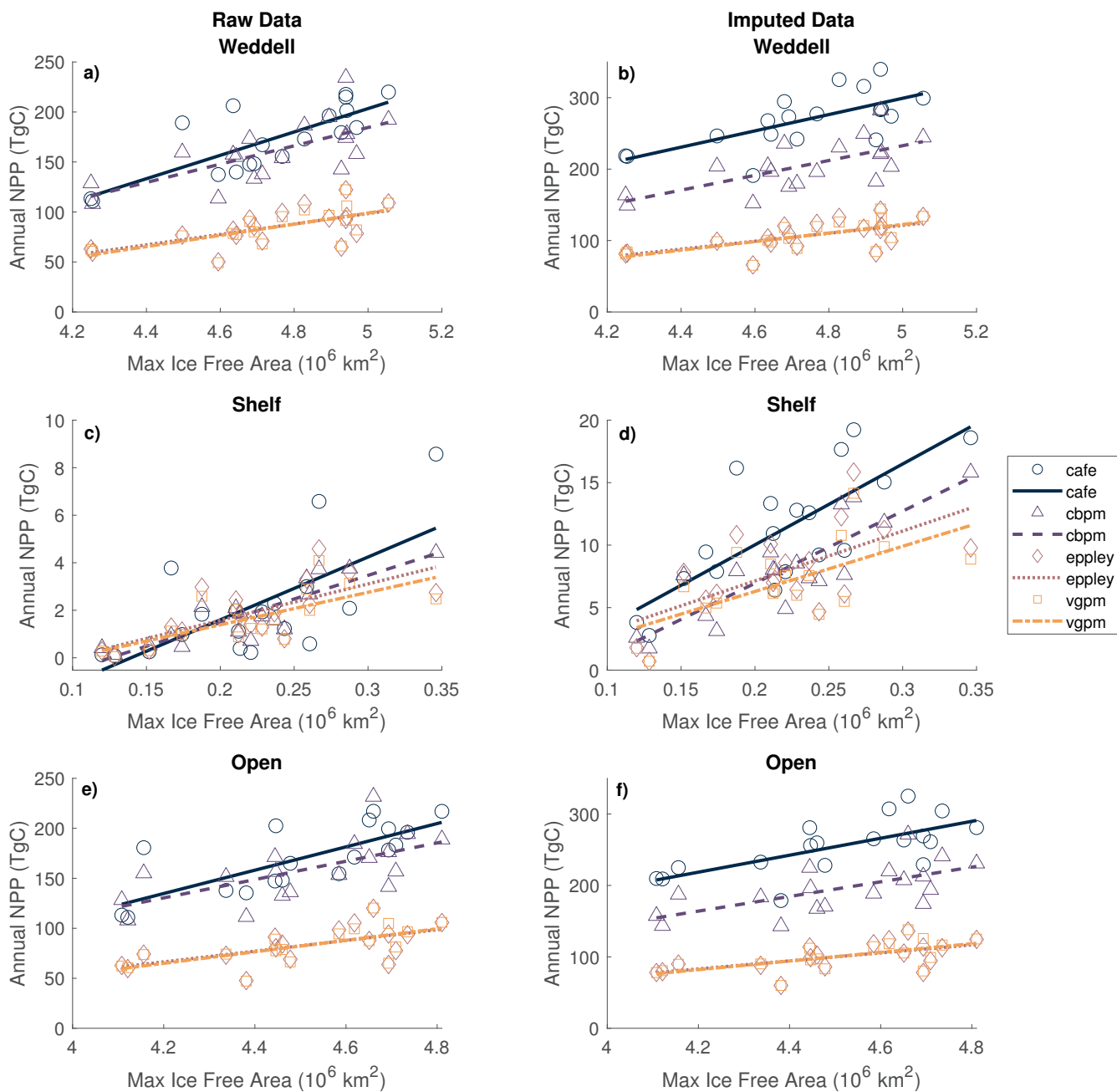


**Figure A3.** Relationship between annual maximum ice-free area and annual NPP for all four NPP models for the entire Weddell Gyre (a-b), Shelf region (c-d) and Open Ocean region (e-f). Panels a), c) and e) show the regressions using the directly-observed raw estimates of total annual NPP. Panels b), d) and f) show the regressions using the imputed annual NPP estimates.

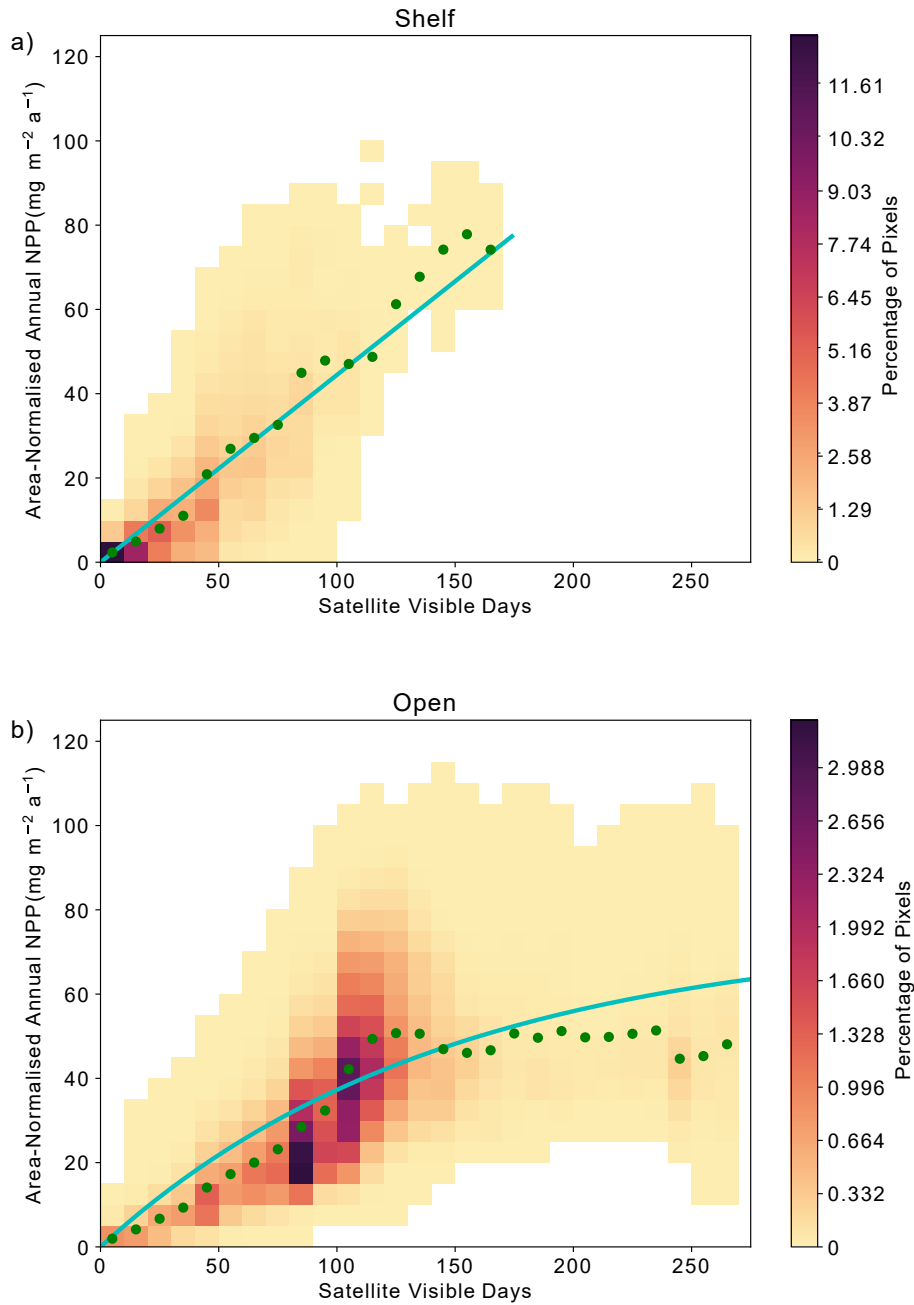


**Figure A4.** Chlorophyll-a concentration-Relationship between 0-200m-area-normalised annual NPP and number of visible days (VD) for each float found within all satellite data pixels over the Weddell Gyre study region between 2014-2021 timeseries as reported in the CbPM NPP product. Black line represents Heatmap shows the mixed layer depth area-normalised density distribution of data points, while the lines show the (a) linear (shelf) and shaded areas represent (b) non-linear (open ocean) relationships for the whole timeseries. VD bin means are plotted in green.

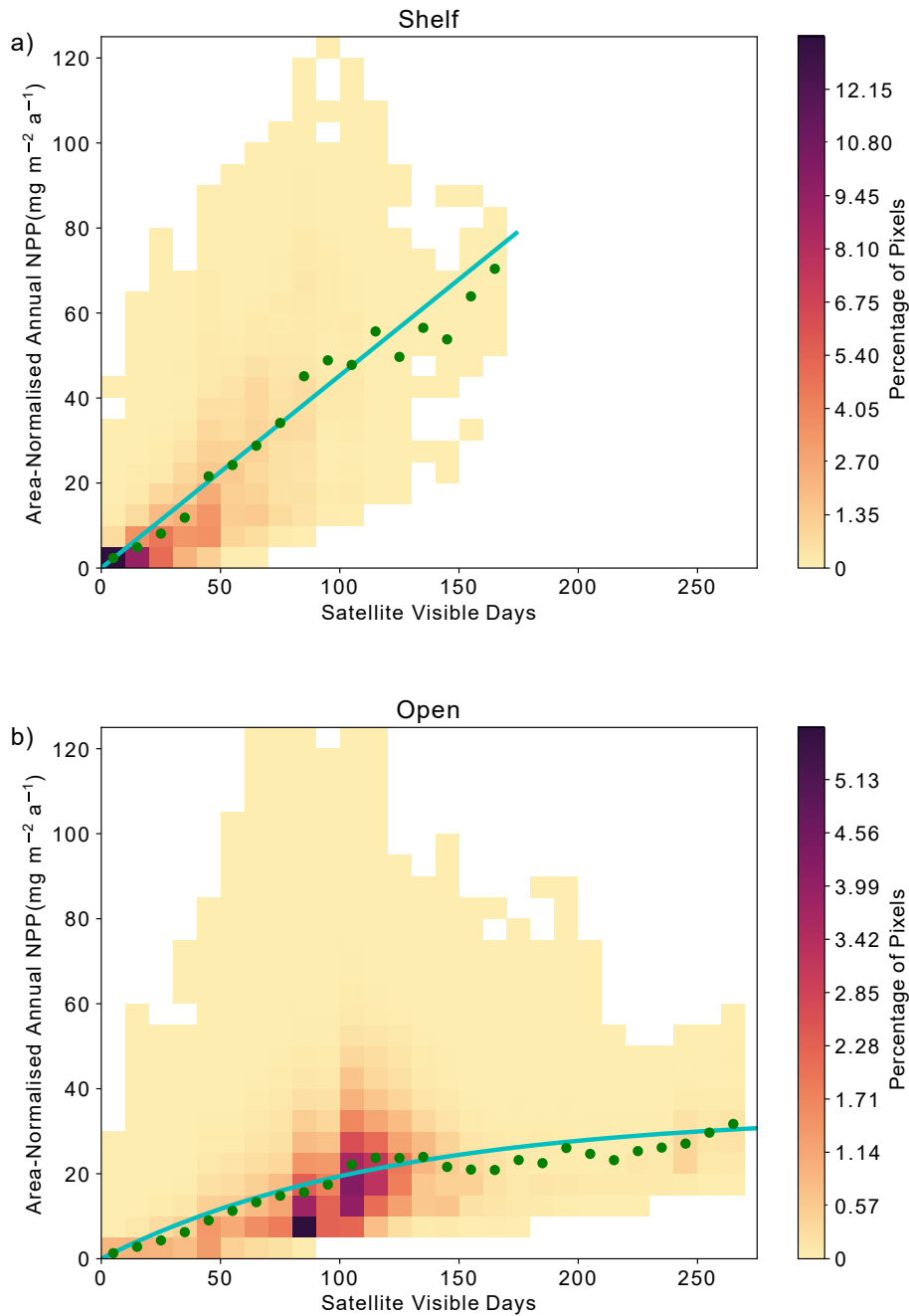


**Figure A5.** Relationship between area-normalised annual NPP and number of visible days (VD) for all satellite data extrapolated to pixels over the surface from timeseries as reported in the shallowest float measurement VGPM-Eppley NPP product. Note colour scales vary between floats. Heatmap shows the area-normalised density distribution of data points, while the lines show the (a) linear (shelf) and (b) non-linear (open ocean) relationships for the whole timeseries. VD bin means are plotted in green.

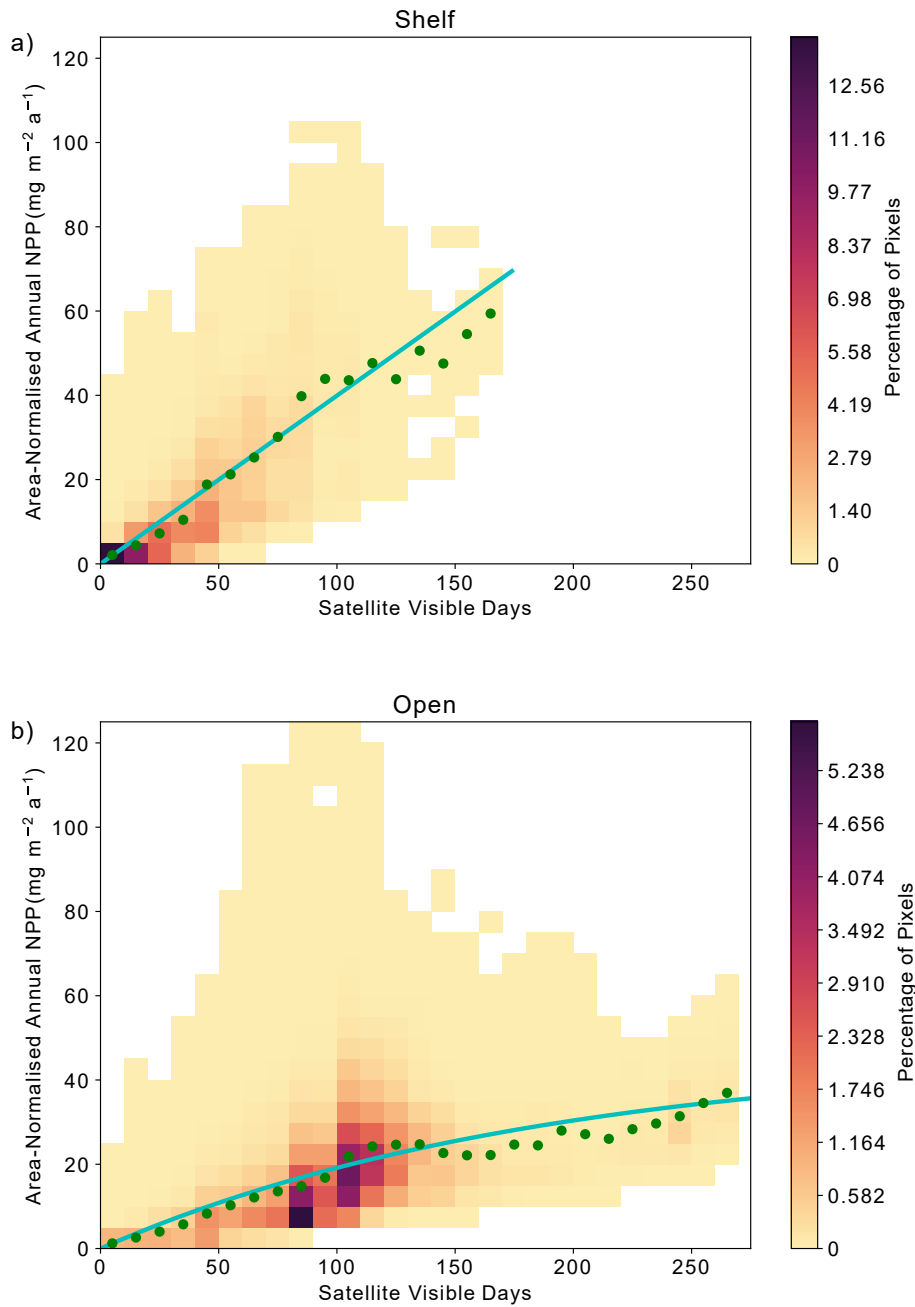


**Figure A6.** Relationship between area-normalised annual NPP and number of visible days (VD) for all satellite data pixels over the timeseries as reported in the VGPM NPP product. Heatmap shows the area-normalised density distribution of data points, while the lines show the (a) linear (shelf) and (b) non-linear (open ocean) relationships for the whole timeseries. VD bin means are plotted in green.



*Acknowledgements.* This work was supported by the Natural Environmental Research Council (~~grant numbers~~ NE/S007210/1 ~~and~~ ~~&~~ NE/X008657/1) and by a European Research Council Consolidator grant (GOCART, agreement no. 724416). GAM was supported by the NSF-funded SOC-COM project (PLR-1425989) and UKRI (MR/W013835/1).

## References

- 635 Akhoudas, C. H., Sallée, J. B., Haumann, F. A., Meredith, M. P., Garabato, A. N., Reverdin, G., Jullion, L., Aloisi, G., Benetti, M., Leng, M. J., and Arrowsmith, C.: Ventilation of the abyss in the Atlantic sector of the Southern Ocean, *Scientific reports*, 11, <https://doi.org/10.1038/S41598-021-86043-2>, 2021.
- Ardyna, M., Claustre, H., Sallée, J. B., D'Ovidio, F., Gentili, B., van Dijken, G., D'Ortenzio, F., and Arrigo, K. R.: Delineating environmental control of phytoplankton biomass and phenology in the Southern Ocean, *Geophysical Research Letters*, 44, 5016–5024, <https://doi.org/10.1002/2016GL072428>, 2017.
- 640 Arrigo, K. R. and van Dijken, G. L.: Annual cycles of sea ice and phytoplankton in Cape Bathurst polynya, southeastern Beaufort Sea, Canadian Arctic, *Geophysical Research Letters*, 31, 2–5, <https://doi.org/10.1029/2003GL018978>, 2004.
- Arrigo, K. R. and Van Dijken, G. L.: Secular trends in Arctic Ocean net primary production, *Journal of Geophysical Research: Oceans*, 116, <https://doi.org/10.1029/2011JC007151>, 2011.
- 645 Arrigo, K. R., van Dijken, G., and Long, M.: Coastal Southern Ocean: A strong anthropogenic CO<sub>2</sub> sink, *Geophysical Research Letters*, 35, 1–6, <https://doi.org/10.1029/2008GL035624>, 2008a.
- Arrigo, K. R., van Dijken, G. L., and Bushinsky, S.: Primary production in the Southern Ocean, 1997–2006, *Journal of Geophysical Research: Oceans*, 113, 1997–2006, <https://doi.org/10.1029/2007JC004551>, 2008b.
- Arrigo, K. R., Van Dijken, G. L., and Strong, A. L.: Environmental controls of marine productivity hot spots around Antarctica, *Journal of Geophysical Research: Oceans*, 120, 5545–5565, <https://doi.org/10.1002/2015JC010888>, 2015.
- 650 Arteaga, L. A., Pahlow, M., Bushinsky, S. M., and Sarmiento, J. L.: Nutrient Controls on Export Production in the Southern Ocean, *Global Biogeochemical Cycles*, 33, 942–956, <https://doi.org/10.1029/2019GB006236>, 2019.
- Arteaga, L. A., Boss, E., Behrenfeld, M. J., Westberry, T. K., and Sarmiento, J. L.: Seasonal modulation of phytoplankton biomass in the Southern Ocean, *Nature Communications*, 11, 1–10, <https://doi.org/10.1038/s41467-020-19157-2>, 2020.
- 655 Bacon, S. and Jullion, L.: RRS James Cook: Antarctic deep water rates of export (ANDREX), Tech. rep., National Oceanography Centre, 2009.
- Baldry, K., Strutton, P. G., Hill, N. A., and Boyd, P. W.: Subsurface Chlorophyll-a Maxima in the Southern Ocean, *Frontiers in Marine Science*, 7, <https://doi.org/10.3389/fmars.2020.00671>, 2020.
- Behrenfeld, M. J. and Falkowski, P. G.: Photosynthetic rates derived from satellite-based chlorophyll concentration, *Limnology and Oceanography*, 42, 1–20, <https://doi.org/10.4319/lo.1997.42.1.0001>, 1997.
- 660 Behrenfeld, M. J., Boss, E., Siegel, D. A., and Shea, D. M.: Carbon-based ocean productivity and phytoplankton physiology from space, *Global Biogeochemical Cycles*, 19, 1–14, <https://doi.org/10.1029/2004GB002299>, 2005.
- Biddle, L. C. and Swart, S.: The Observed Seasonal Cycle of Submesoscale Processes in the Antarctic Marginal Ice Zone, *Journal of Geophysical Research: Oceans*, 125, <https://doi.org/10.1029/2019JC015587>, 2020.
- 665 Bisson, K. M. and Cael, B. B.: How Are Under Ice Phytoplankton Related to Sea Ice in the Southern Ocean?, *Geophysical Research Letters*, 48, e2021GL095051, <https://doi.org/10.1029/2021GL095051>, 2021.
- Boyd, P. W., Arrigo, K. R., Strzepek, R., and Van Dijken, G. L.: Mapping phytoplankton iron utilization: Insights into Southern Ocean supply mechanisms, *J. Geophys. Res.*, 117, 6009, <https://doi.org/10.1029/2011JC007726>, 2012.
- Boyd, P. W., Claustre, H., Levy, M., Siegel, D. A., and Weber, T.: Multi-faceted particle pumps drive carbon sequestration in the ocean, *Nature*, 568, 327–335, <https://doi.org/10.1038/s41586-019-1098-2>, 2019.
- 670

- Briggs, E. M., Martz, T. R., Talley, L. D., Mazloff, M. R., and Johnson, K. S.: Physical and Biological Drivers of Biogeochemical Tracers Within the Seasonal Sea Ice Zone of the Southern Ocean From Profiling Floats, *Journal of Geophysical Research: Oceans*, 123, 746–758, <https://doi.org/10.1002/2017JC012846>, 2018.
- 675 Briggs, N., Perry, M. J., Cetinić, I., Lee, C., D’Asaro, E., Gray, A. M., and Rehm, E.: High-resolution observations of aggregate flux during a sub-polar North Atlantic spring bloom, *Deep-Sea Research Part I: Oceanographic Research Papers*, 58, 1031–1039, <https://doi.org/10.1016/j.dsr.2011.07.007>, 2011.
- Bronselaeer, B., Russell, J. L., Winton, M., Williams, N. L., Key, R. M., Dunne, J. P., Feely, R. A., Johnson, K. S., and Sarmiento, J. L.: Importance of wind and meltwater for observed chemical and physical changes in the Southern Ocean, *Nature Geoscience* 2020 13:1, 13, 35–42, <https://doi.org/10.1038/s41561-019-0502-8>, 2020.
- 680 Brown, P. J., Meredith, M. P., Jullion, L., Garabato, A. N., Torres-Valdés, S., Holland, P., Leng, M. J., and Venables, H.: Freshwater fluxes in the Weddell Gyre: results from  $\delta^{18}\text{O}$ , *Philosophical transactions. Series A, Mathematical, physical, and engineering sciences*, 372, <https://doi.org/10.1098/RSTA.2013.0298>, 2014.
- Brown, P. J., Jullion, L., Landschützer, P., Bakker, D. C., Naveira Garabato, A. C., Meredith, M. P., Torres-Valdés, S., Watson, A. J., Hoppema, M., Loose, B., Jones, E. M., Telszewski, M., Jones, S. D., and Wanninkhof, R.: Carbon dynamics of the Weddell Gyre, Southern Ocean, *Global Biogeochemical Cycles*, 29, 288–306, <https://doi.org/10.1002/2014GB005006>, 2015.
- 685 Buchovecky, B., MacGilchrist, G. A., Bushuk, M., Haumann, F. A., Frölicher, T. L., Le Grix, N., and Dunne, J.: Potential Predictability of the Spring Bloom in the Southern Ocean Sea Ice Zone, *Geophysical Research Letters*, 50, e2023GL105139, <https://doi.org/10.1029/2023GL105139>, 2023.
- Bushinsky, S. M., Landschützer, P., Rödenbeck, C., Gray, A. R., Baker, D., Mazloff, M. R., Resplandy, L., Johnson, K. S., and Sarmiento, J. L.: Reassessing Southern Ocean Air-Sea CO<sub>2</sub> Flux Estimates With the Addition of Biogeochemical Float Observations, *Global Biogeochemical Cycles*, 33, 1370–1388, <https://doi.org/10.1029/2019GB006176>, 2019.
- 690 Bushuk, M., Winton, M., Haumann, F. A., Delworth, T., Lu, F., Zhang, Y., Jia, L., Zhang, L., Cooke, W., Harrison, M., Hurlin, B., Johnson, N. C., Kapnick, S. B., McHugh, C., Murakami, H., Rosati, A., Tseng, K. C., Wittenberg, A. T., Yang, X., and Zeng, F.: Seasonal prediction and predictability of regional antarctic Sea ice, *Journal of Climate*, 34, 6207–6233, <https://doi.org/10.1175/JCLI-D-20-0965.1>, 2021.
- 695 Campbell, E. C., Wilson, E. A., Kent Moore, G. W., Riser, S. C., Brayton, C. E., Mazloff, M. R., and Talley, L. D.: Antarctic offshore polynyas linked to Southern Hemisphere climate anomalies, *Nature*, 570, 319–325, <https://doi.org/10.1038/s41586-019-1294-0>, 2019.
- Casagrande, F., Stachelski, L., and de Souza, R. B.: Assessment of Antarctic sea ice area and concentration in Coupled Model Intercomparison Project Phase 5 and Phase 6 models, *International Journal of Climatology*, <https://doi.org/10.1002/joc.7916>, 2023.
- de Baar, H. J., Bathmann, U., Smetacek, V., Löscher, B. M., and Veth, C.: Importance of iron for plankton blooms and carbon dioxide drawdown in the Southern Ocean, *Nature*, 373, 412–415, <https://doi.org/10.1038/373412a0>, 1995.
- 700 Ducklow, H. W., Stukel, M. R., Eveleth, R., Doney, S. C., Jickells, T., Schofield, O., Baker, A. R., Brindle, J., Chance, R., and Cassar, N.: Spring-summer net community production, new production, particle export and related water column biogeochemical processes in the marginal sea ice zone of the Western Antarctic Peninsula 2012–2014, *Philosophical Transactions of the Royal Society A: Mathematical, Physical and Engineering Sciences*, 376, 20170177, <https://doi.org/10.1098/rsta.2017.0177>, 2018.
- 705 Eppley, R. W.: Temperature and phytoplankton growth in the sea, *Fishery Bulletin*, 70, 1063–1085, 1972.
- Geibert, W., Assmy, P., Bakker, D. C., Hanfland, C., Hoppema, M., Pichevin, L. E., Schröder, M., Schwarz, J. N., Stimac, I., Usbeck, R., and Webb, A.: High productivity in an ice melting hot spot at the eastern boundary of the Weddell Gyre, *Global Biogeochemical Cycles*, 24, <https://doi.org/10.1029/2009GB003657>, 2010.

- Giddy, I., Nicholson, S., Queste, B., Thomalla, S., and Swart, S.: Sea-ice impacts inter-annual variability in phytoplankton phenology and carbon export in the Weddell Sea, *Geophysical Research Letters*, 50, e2023GL103695, <https://doi.org/10.1029/2023GL103695>, 2023.
- 710 Gordon, H. R. and McCluney, W. R.: Estimation of the Depth of Sunlight Penetration in the Sea for Remote Sensing, *Applied Optics*, Vol. 14, Issue 2, pp. 413-416, 14, 413–416, <https://doi.org/10.1364/AO.14.000413>, 1975.
- Gupta, M., Follows, M. J., and Lauderdale, J. M.: The Effect of Antarctic Sea Ice on Southern Ocean Carbon Outgassing: Capping Versus Light Attenuation, *Global Biogeochemical Cycles*, 34, <https://doi.org/10.1029/2019GB006489>, 2020.
- 715 Hague, M. and Vichi, M.: Southern Ocean Biogeochemical Argo detect under-ice phytoplankton growth before sea ice retreat, *Biogeosciences*, 18, 25–38, <https://doi.org/10.5194/bg-18-25-2021>, 2021.
- Hauck, J., Völker, C., Wolf-Gladrow, D. A., Laufkötter, C., Vogt, M., Aumont, O., Bopp, L., Buitenhuis, E. T., Doney, S. C., Dunne, J., Gruber, N., Hashioka, T., John, J., Quéré, C. L., Lima, I. D., Nakano, H., Séférian, R., and Totterdell, I.: On the Southern Ocean CO<sub>2</sub> uptake and the role of the biological carbon pump in the 21st century, *Global Biogeochemical Cycles*, 29, 1451–1470, <https://doi.org/10.1002/2015GB005140>, 2015.
- 720 Hawco, N. J., Tagliabue, A., and Twining, B. S.: Manganese Limitation of Phytoplankton Physiology and Productivity in the Southern Ocean, *Global Biogeochemical Cycles*, 36, <https://doi.org/10.1029/2022GB007382>, 2022.
- Henley, S., Cavan, E. L., Fawcett, S. E., Kerr, R., Monteiro, T., Sherrell, R. M., Bowie, A. R., Boyd, P. W., Barnes, D. K. A., Schloss, I. R., Marshall, T., Flynn, R., and Smith, S.: Changing Biogeochemistry of the Southern Ocean and Its Ecosystem Implications, *Frontiers in Marine Science*, 581, <https://doi.org/10.3389/fmars.2020.00581>, 2020.
- 725 Henson, S. A., Laufkötter, C., Leung, S., Giering, S. L., Palevsky, H. I., and Cavan, E. L.: Uncertain response of ocean biological carbon export in a changing world, *Nature Geoscience* 2022 15:4, 15, 248–254, <https://doi.org/10.1038/s41561-022-00927-0>, 2022.
- Hindell, M. A., Reisinger, R. R., Ropert-Coudert, Y., Hückstädt, L. A., Trathan, P. N., Bornemann, H., Charrassin, J. B., Chown, S. L., Costa, D. P., Danis, B., Lea, M. A., Thompson, D., Torres, L. G., Van de Putte, A. P., Alderman, R., Andrews-Goff, V., Arthur, B., Ballard, G., Bengtson, J., Bester, M. N., Blix, A. S., Boehme, L., Bost, C. A., Boveng, P., Cleeland, J., Constantine, R., Corney, S., Crawford, R. J., Dalla Rosa, L., de Bruyn, P. J., Delord, K., Descamps, S., Double, M., Emmerson, L., Fedak, M., Friedlaender, A., Gales, N., Goebel, M. E., Goetz, K. T., Guinet, C., Goldsworthy, S. D., Harcourt, R., Hinke, J. T., Jerosch, K., Kato, A., Kerry, K. R., Kirkwood, R., Kooyman, G. L., Kovacs, K. M., Lawton, K., Lowther, A. D., Lydersen, C., Lyver, P. O., Makhado, A. B., Márquez, M. E., McDonald, B. I., McMahon, C. R., Muelbert, M., Nachtsheim, D., Nicholls, K. W., Nordøy, E. S., Olmastroni, S., Phillips, R. A., Pistorius, P., Plötz, J., Pütz, K., Ratcliffe, N., Ryan, P. G., Santos, M., Southwell, C., Staniland, I., Takahashi, A., Tarroux, A., Trivelpiece, W., Wakefield, E., Weimerskirch, H., Wienecke, B., Xavier, J. C., Wotherspoon, S., Jonsen, I. D., and Raymond, B.: Tracking of marine predators to protect Southern Ocean ecosystems, *Nature*, 580, 87–92, <https://doi.org/10.1038/s41586-020-2126-y>, 2020.
- 735 Hoppema, M.: Weddell Sea is a globally significant contributor to deep-sea sequestration of natural carbon dioxide, *Deep-Sea Research Part I: Oceanographic Research Papers*, 51, 1169–1177, <https://doi.org/10.1016/j.dsr.2004.02.011>, 2004.
- 740 Hoppema, M., Goeyens, L., and Fahrbach, E.: Intense nutrient removal in the remote area off Larsen Ice Shelf (Weddell Sea), *Polar Biology*, 23, 85–94, 2000.
- Hoppema, M., Middag, R., De Baar, H. J., Fahrbach, E., Van Weerlee, E. M., and Thomas, H.: Whole season net community production in the Weddell Sea, *Polar Biology*, 31, 101–111, <https://doi.org/10.1007/s00300-007-0336-5>, 2007.
- Hoppema, M., Bakker, K., van Heuven, S. M., van Ooijen, J. C., and de Baar, H. J.: Distributions, trends and inter-annual variability of nutrients along a repeat section through the Weddell Sea (1996-2011), *Marine Chemistry*, 177, 545–553, <https://doi.org/10.1016/j.marchem.2015.08.007>, 2015.
- 745

- Johnson, K. S., Plant, J. N., Coletti, L. J., Jannasch, H. W., Sakamoto, C. M., Riser, S. C., Swift, D. D., Williams, N. L., Boss, E., Haëntjens, N., Talley, L. D., and Sarmiento, J. L.: Biogeochemical sensor performance in the SOCCOM profiling float array, *Journal of Geophysical Research: Oceans*, 122, 6416–6436, <https://doi.org/10.1002/2017JC012838>, 2017.
- 750 Jullion, L., Garabato, A. C., Bacon, S., Meredith, M. P., Brown, P. J., Torres-Valdés, S., Speer, K. G., Holland, P. R., Dong, J., Bakker, D., Hoppema, M., Loose, B., Venables, H. J., Jenkins, W. J., Messias, M. J., and Fahrbach, E.: The contribution of the Weddell Gyre to the lower limb of the Global Overturning Circulation, *Journal of Geophysical Research: Oceans*, 119, 3357–3377, <https://doi.org/10.1002/2013JC009725>, 2014.
- 755 Kauko, H. M., Assmy, P., Peeken, I., Róžańska-Pluta, M., Wiktor, J. M., Bratbak, G., Singh, A., Ryan-Keogh, T. J., and Moreau, S.: First phytoplankton community assessment of the Kong Håkon VII Hav, Southern Ocean, during austral autumn, *Biogeosciences*, 19, 5449–5482, <https://doi.org/10.5194/bg-19-5449-2022>, 2022.
- Kim, S.-U. and Kim, K.-Y.: Impact of climate change on the primary production and related biogeochemical cycles in the coastal and sea ice zone of the Southern Ocean, *Science of the Total Environment*, 751, <https://doi.org/10.1016/j.scitotenv.2020.141678>, 2021.
- 760 Klatt, O., Boebel, O., and Fahrbach, E.: A profiling float’s sense of ice, *Journal of Atmospheric and Oceanic Technology*, 24, 1301–1308, <https://doi.org/10.1175/JTECH2026.1>, 2007.
- Kumar, A., Yadav, J., and Mohan, R.: Seasonal sea-ice variability and its trend in the Weddell Sea sector of West Antarctica, *Environmental Research Letters*, 16, 024 046, <https://doi.org/10.1088/1748-9326/abdc88>, 2021.
- 765 Lafond, A., Leblanc, K., Legras, J., Cornet, V., and Quéguiner, B.: The structure of diatom communities constrains biogeochemical properties in surface waters of the Southern Ocean (Kerguelen Plateau), *Journal of Marine Systems*, 212, <https://doi.org/10.1016/j.jmarsys.2020.103458>, 2020.
- Libera, S., Hobbs, W., Klocker, A., Meyer, A., and Matear, R.: Ocean-Sea Ice Processes and Their Role in Multi-Month Predictability of Antarctic Sea Ice, *Geophysical Research Letters*, 49, 1–10, <https://doi.org/10.1029/2021GL097047>, 2022.
- 770 Lin, Y., Moreno, C., Marchetti, A., Ducklow, H., Schofield, O., Delage, E., Meredith, M., Li, Z., Eveillard, D., Chaffron, S., and Cassar, N.: Decline in plankton diversity and carbon flux with reduced sea ice extent along the Western Antarctic Peninsula, *Nature Communications* 2021 12:1, 12, 1–9, <https://doi.org/10.1038/s41467-021-25235-w>, 2021.
- Ludescher, J., Yuan, N., and Bunde, A.: Detecting the statistical significance of the trends in the Antarctic sea ice extent: an indication for a turning point, *Climate Dynamics*, 53, 237–244, <https://doi.org/10.1007/s00382-018-4579-3>, 2019.
- 775 MacGilchrist, G. A., Naveira Garabato, A. C., Brown, P. J., Jullion, L., Bacon, S., Bakker, D. C., Hoppema, M., Meredith, M. P., and Torres-Valdés, S.: Reframing the carbon cycle of the subpolar Southern Ocean, *Science Advances*, 5, eaav6410, <https://doi.org/10.1126/sciadv.aav6410>, 2019.
- Mascioni, M., Almandoz, G. O., Ekern, L., Pan, B. J., and Vernet, M.: Microplanktonic diatom assemblages dominated the primary production but not the biomass in an Antarctic fjord, *Journal of Marine Systems*, 224, 103 624, <https://doi.org/10.1016/J.JMARSYS.2021.103624>, 2021.
- 780 McClish, S. and Bushinsky, S. M.: Majority of Southern Ocean Seasonal Sea Ice Zone Bloom Net Community Production Precedes Total Ice Retreat, *Geophysical Research Letters*, 50, e2023GL103 459, <https://doi.org/10.1029/2023GL103459>, 2023.
- McGillicuddy, D. J., Sedwick, P. N., Dinniman, M. S., Arrigo, K. R., Bibby, T. S., Greenan, B. J., Hofmann, E. E., Klinck, J. M., Smith, W. O., Mack, S. L., Marsay, C. M., Sohst, B. M., and Van Dijken, G. L.: Iron supply and demand in an Antarctic shelf ecosystem, *Geophysical Research Letters*, 42, 8088–8097, <https://doi.org/10.1002/2015GL065727>, 2015.

- Meier, W. N., Fetterer, F., Windnagel, A. K., and Stewart, J. S.: NOAA/NSIDC Climate Data Record of Passive Microwave Sea Ice Concentration, Version 4. 2002–2021, 2021.
- 785 Meredith, M., Sommerkorn, M., Cassotta, S., Derksen, C., Ekaykin, A., Hollowed, A., Kofinas, G., Mackintosh, A., Melbourne-Thomas, J., Muelbert, M., Ottersen, G., Pritchard, H., and Schuur, E.: Polar Regions, in: *The Ocean and Cryosphere in a Changing Climate*, edited by Pörtner, H.-O., Roberts, D., Masson-Delmotte, V., Zhai, P., Tignor, M., Poloczanska, E., Mintenbeck, K., Alegría, A., Nicolai, M., Okem, A., Petzold, J., Rama, B., and Weyer, N., pp. 203–320, Cambridge University Press, <https://doi.org/10.1017/9781009157964.005>, 2019.
- 790 Meredith, M. P.: Cruise report: RRS James Clark Ross JR235/236/239, Tech. rep., British Antarctic Survey, 2010.
- Meredith, M. P., Jullion, L., Brown, P. J., Garabato, A. C., and Couldrey, M. P.: Dense waters of the Weddell and Scotia seas: Recent changes in properties and circulation, <https://doi.org/10.1098/rsta.2013.0041>, 2014.
- Moreau, S., Hattermann, T., de Steur, L., Kauko, H. M., Ahonen, H., Ardelan, M., Assmy, P., Chierici, M., Descamps, S., Dinter, T., Falkenhaus, T., Fransson, A., Grønningsæter, E., Hallfredsson, E. H., Huhn, O., Lebrun, A., Lowther, A., Lübcker, N., Monteiro, P., 795 Peeken, I., Roychoudhury, A., Róžańska, M., Ryan-Keogh, T., Sanchez, N., Singh, A., Simonsen, J. H., Steiger, N., Thomalla, S. J., van Tonder, A., Wiktor, J. M., and Steen, H.: Wind-driven upwelling of iron sustains dense blooms and food webs in the eastern Weddell Gyre, *Nature Communications*, 14, 1303, <https://doi.org/10.1038/s41467-023-36992-1>, 2023.
- Morel, A.: Light and marine photosynthesis: A spectral model with geochemical and climatological implications, *Progress in Oceanography*, 26, 263–306, 1991.
- 800 National Geophysical Data Center/NESDIS/NOAA/U.S. Department of Commerce.: TerrainBase, Global 5 Arc-minute Ocean Depth and Land Elevation from the US National Geophysical Data Center (NGDC)., Research Data Archive at the National Center for Atmospheric Research, Computational and Information Systems Laboratory, Accessed 1, <https://doi.org/https://doi.org/10.5065/E08M-4482>., 1995.
- Nissen, C., Timmermann, R., Hoppema, M., Gürses, , and Hauck, J.: Abruptly attenuated carbon sequestration with Weddell Sea dense waters by 2100, *Nature Communications*, 13, <https://doi.org/10.1038/s41467-022-30671-3>, 2022.
- 805 Noh, K. M., Lim, H. G., Yang, E. J., and Kug, J. S.: Emergent Constraint for Future Decline in Arctic Phytoplankton Concentration, *Earth's Future*, 11, <https://doi.org/10.1029/2022EF003427>, 2023.
- Park, J., Kuzminov, F. I., Bailleul, B., Yang, E. J., Lee, S. H., Falkowski, P. G., and Gorbunov, M. Y.: Light availability rather than Fe controls the magnitude of massive phytoplankton bloom in the Amundsen Sea polynyas, Antarctica, *Limnology and Oceanography*, 62, 2260–2276, <https://doi.org/10.1002/LNO.10565>, 2017.
- 810 Peck, L. S., Barnes, D. K., Cook, A. J., Fleming, A. H., and Clarke, A.: Negative feedback in the cold: Ice retreat produces new carbon sinks in Antarctica, *Global Change Biology*, 16, 2614–2623, <https://doi.org/10.1111/j.1365-2486.2009.02071.x>, 2010.
- Pinkerton, M. H., Boyd, P. W., Deppeler, S., Hayward, A., Höfer, J., and Moreau, S.: Evidence for the Impact of Climate Change on Primary Producers in the Southern Ocean, *Frontiers in Ecology and Evolution*, 9, 134, <https://doi.org/10.3389/fevo.2021.592027>, 2021.
- Pope, A., Wagner, P., Johnson, R., Shutler, J. D., Baeseman, J., and Newman, L.: Community review of Southern Ocean satellite data needs, 815 *Antarctic Science*, 29, 97–138, <https://doi.org/10.1017/S0954102016000390>, 2017.
- Prend, C. J., Keerthi, M. G., Lévy, M., Aumont, O., Gille, S. T., and Talley, L. D.: Sub-Seasonal Forcing Drives Year-To-Year Variations of Southern Ocean Primary Productivity, *Global Biogeochemical Cycles*, 36, <https://doi.org/10.1029/2022GB007329>, 2022.
- Quéguiner, B.: Iron fertilization and the structure of planktonic communities in high nutrient regions of the Southern Ocean, *Deep Sea Research Part II: Topical Studies in Oceanography*, 90, 43–54, <https://doi.org/10.1016/J.DSR2.2012.07.024>, 2013.

- 820 Rohr, T., Long, M. C., Kavanaugh, M. T., Lindsay, K., and Doney, S. C.: Variability in the mechanisms controlling Southern Ocean phytoplankton bloom phenology in an ocean model and satellite observations, *Global Biogeochemical Cycles*, 31, 922–940, <https://doi.org/10.1002/2016GB005615>, 2017.
- Ryan-Keogh, T. J., DeLizo, L. M., Smith, W. O., Sedwick, P. N., McGillicuddy, D. J., Moore, C. M., and Bibby, T. S.: Temporal progression of photosynthetic-strategy in phytoplankton in the Ross Sea, Antarctica, *Journal of Marine Systems*, 166, 87–96, 825 <https://doi.org/10.1016/j.jmarsys.2016.08.014>, 2017.
- Ryan-keogh, T. J., Thomalla, S. J., Chang, N., and Moalusi, T.: A new global oceanic multi-model net primary productivity data product, *Earth Syst. Sci. Data Discuss.*, In review, 1–34, 2023.
- Schultz, C., Doney, S. C., Hauck, J., Kavanaugh, M. T., and Schofield, O.: Modeling Phytoplankton Blooms and Inorganic Carbon Responses to Sea-Ice Variability in the West Antarctic Peninsula, *Journal of Geophysical Research: Biogeosciences*, 126, e2020JG006227, 830 <https://doi.org/10.1029/2020JG006227>, 2021.
- Sedwick, P. N. and Ditullio, G. R.: Regulation of algal blooms in Antarctic shelf waters by the release of iron from melting sea ice, *Geophysical Research Letters*, 24, 2515–2518, <https://doi.org/10.1029/97GL02596>, 1997.
- Sedwick, P. N., Marsay, C. M., Sohst, B. M., Aguilar-Islas, A. M., Lohan, M. C., Long, M. C., Arrigo, K. R., Dunbar, R. B., Saito, M. A., Smith, W. O., and Ditullio, G. R.: Early season depletion of dissolved iron in the Ross Sea polynya: Implications for iron dynamics on the 835 Antarctic continental shelf, *Journal of Geophysical Research: Oceans*, 116, <https://doi.org/10.1029/2010JC006553>, 2011.
- Séférian, R., Berthet, S., Yool, A., Palmiéri, J., Bopp, L., Tagliabue, A., Kwiatkowski, L., Aumont, O., Christian, J., Dunne, J., Gehlen, M., Ilyina, T., John, J. G., Li, H., Long, M. C., Luo, J. Y., Nakano, H., Romanou, A., Schwinger, J., Stock, C., Santana-Falcón, Y., Takano, Y., Tjiputra, J., Tsujino, H., Watanabe, M., Wu, T., Wu, F., and Yamamoto, A.: Tracking Improvement in Simulated Marine Biogeochemistry Between CMIP5 and CMIP6, *Current Climate Change Reports*, 6, 95–119, <https://doi.org/10.1007/s40641-020-00160-0>, 2020.
- 840 Sigman, D. M., Hain, M. P., and Haug, G. H.: The polar ocean and glacial cycles in atmospheric CO<sub>2</sub> concentration, *Nature*, 466, 47–55, <https://doi.org/10.1038/nature09149>, 2010.
- Silsbe, G. M., Behrenfeld, M. J., Halsey, K. H., Milligan, A. J., and Westberry, T. K.: The CAFE model: A net production model for global ocean phytoplankton, *Global Biogeochemical Cycles*, 30, 1756–1777, <https://doi.org/10.1002/2016GB005521>, 2016.
- Smetacek, V., Assmy, P., and Henjes, J.: The role of grazing in structuring Southern Ocean pelagic ecosystems and biogeochemical cycles, 845 *Antarctic Science*, 16, 541–558, <https://doi.org/10.1017/S0954102004002317>, 2004.
- Smith, W. O. and Comiso, J. C.: Influence of sea ice on primary production in the Southern Ocean: A satellite perspective, *Journal of Geophysical Research: Oceans*, 113, 1–19, <https://doi.org/10.1029/2007JC004251>, 2008.
- Speer, K. G. and Dittmar, T.: Cruise report, RV Revelle, 33RR20080204, Tech. rep., Florida State University, 2008.
- Swart, S., Plessis, M. D., Thompson, A. F., Biddle, L. C., Giddy, I., Linders, T., Mohrmann, M., and Nicholson, S.: Submesoscale Fronts in the Antarctic Marginal Ice Zone and Their Response to Wind Forcing, *Geophysical Research Letters*, 47, 850 <https://doi.org/10.1029/2019GL086649>, 2020.
- Takao, S., Nakaoka, S. I., Hashihama, F., Shimada, K., Yoshikawa-Inoue, H., Hirawake, T., Kanda, J., Hashida, G., and Suzuki, K.: Effects of phytoplankton community composition and productivity on sea surface pCO<sub>2</sub> variations in the Southern Ocean, *Deep-Sea Research Part I: Oceanographic Research Papers*, 160, <https://doi.org/10.1016/j.dsr.2020.103263>, 2020.
- 855 Taylor, M. H., Losch, M., and Bracher, A.: On the drivers of phytoplankton blooms in the Antarctic marginal ice zone: A modeling approach, *Journal of Geophysical Research: Oceans*, 118, 63–75, <https://doi.org/10.1029/2012JC008418>, 2013.



- Thomalla, S. J., Ogunkoya, A. G., Vichi, M., and Swart, S.: Using optical sensors on gliders to estimate phytoplankton carbon concentrations and chlorophyll-to-carbon ratios in the Southern Ocean, *Frontiers in Marine Science*, 4, 1–19, <https://doi.org/10.3389/FMARS.2017.00034>, 2017.
- 860 Trebilco, R., Melbourne-Thomas, J., and Constable, A. J.: The policy relevance of Southern Ocean food web structure: Implications of food web change for fisheries, conservation and carbon sequestration, *Marine Policy*, 115, 103–119, <https://doi.org/10.1016/j.marpol.2020.103832>, 2020.
- Trimborn, S., Thoms, S., Bischof, K., and Beszteri, S.: Susceptibility of Two Southern Ocean Phytoplankton Key Species to Iron Limitation and High Light, *Frontiers in Marine Science*, 6, 167, <https://doi.org/10.3389/fmars.2019.00167>, 2019.
- 865 Twelves, A. G., Goldberg, D. N., Henley, S. F., Mazloff, M. R., and Jones, D. C.: Self-Shading and Meltwater Spreading Control the Transition From Light to Iron Limitation in an Antarctic Coastal Polynya, *Journal of Geophysical Research: Oceans*, 126, e2020JC016636, <https://doi.org/10.1029/2020JC016636>, 2021.
- Uchida, T., Balwada, D., Abernathy, R., Prend, C. J., Boss, E., and Gille, S. T.: Southern Ocean Phytoplankton Blooms Observed by Biogeochemical Floats, *Journal of Geophysical Research: Oceans*, 124, 7328–7343, <https://doi.org/10.1029/2019JC015355>, 2019.
- 870 Van Heuven, S. M., Hoppema, M., Jones, E. M., and De Baar, H. J.: Rapid invasion of anthropogenic CO<sub>2</sub> into the deep circulation of the Weddell Gyre, *Philosophical Transactions of the Royal Society A: Mathematical, Physical and Engineering Sciences*, 372, <https://doi.org/10.1098/rsta.2013.0056>, 2014.
- Vernet, M., Geibert, W., Hoppema, M., Brown, P. J., Haas, C., Hellmer, H. H., Jokat, W., Jullion, L., Mazloff, M., Bakker, D. C., Brearley, J. A., Croot, P., Hattermann, T., Hauck, J., Hillenbrand, C. D., Hoppe, C. J., Huhn, O., Koch, B. P., Lechtenfeld, O. J., 875 Meredith, M. P., Naveira Garabato, A. C., Nöthig, E. M., Peeken, I., Rutgers van der Loeff, M. M., Schmidtko, S., Schröder, M., Strass, V. H., Torres-Valdés, S., and Verdy, A.: The Weddell Gyre, Southern Ocean: Present Knowledge and Future Challenges, <https://doi.org/10.1029/2018RG000604>, 2019.
- von Berg, L., Prend, C. J., Campbell, E. C., Mazloff, M. R., Talley, L. D., and Gille, S. T.: Weddell Sea Phytoplankton Blooms Modulated by Sea Ice Variability and Polynya Formation, *Geophysical Research Letters*, 47, <https://doi.org/10.1029/2020GL087954>, 2020.
- 880 Westberry, T., Behrenfeld, M. J., Siegel, D. A., Boss, E., and Westberry, C. : Carbon-based primary productivity modeling with vertically resolved photoacclimation, *Global Biogeochem. Cycles*, 22, 2024, <https://doi.org/10.1029/2007GB003078>, 2008.
- Westberry, T. K. and Behrenfeld, M. J.: Oceanic net primary production, in: *Biophysical Applications of Satellite Remote Sensing*, edited by Hanes, J. M., chap. 8, pp. 205–230, Springer, Berlin, Germany, 2013.
- Westberry, T. K., Silsbe, G. M., and Behrenfeld, M. J.: Gross and net primary production in the global ocean: An ocean color remote sensing 885 perspective, *Earth-Science Reviews*, 237, 104–119, <https://doi.org/10.1016/j.earscirev.2023.104322>, 2023.
- Windnagel, A. K., Meier, W. N., Stewart, J. S., Fetterer, F., and Stafford, T.: NOAA/NSIDC Climate Data Record of Passive Microwave Sea Ice Concentration, Version 4, NSIDC Special Report 20, Boulder CO, <https://nsidc.org/data/g02202/versions/4#anchor-1>, 2021.
- Yager, P., Sherrell, R., Stammerjohn, S., Ducklow, H., Schofield, O., Ingall, E., Wilson, S., Lowry, K., Williams, C., Riemann, L., Bertilsson, S., Alderkamp, A.-C., Dinasquet, J., Logares, R., Richert, I., Sipler, R., Melara, A., Mu, L., Newstead, R., Post, A., Swalethorp, R., and 890 van Dijken, G.: A carbon budget for the Amundsen Sea Polynya, Antarctica: Estimating net community production and export in a highly productive polar ecosystem, *Elementa: Science of the Anthropocene*, 4, <https://doi.org/10.12952/JOURNAL.ELEMENTA.000140>, 2016.